THE ACS VIRGO CLUSTER SURVEY. XIII. SBF DISTANCE CATALOG AND THE THREE-DIMENSIONAL STRUCTURE OF THE VIRGO CLUSTER[1]

SIMONA MEI,[2,3,4] JOHN P. BLAKESLEE,[5] PATRICK CÔTÉ,[6] JOHN L. TONRY,[7] MICHAEL J. WEST,[8,9] LAURA FERRARESE,[6]
ANDRÉS JORDÁN,[10] ERIC W. PENG,[6] ANDRÉ ANTHONY,[6] AND DAVID MERRITT[11]

ABSTRACT

The ACS Virgo Cluster Survey consists of *HST* ACS imaging for 100 early-type galaxies in the Virgo Cluster, observed in the F475W ($\approx$SDSS g) and F850LP ($\approx$SDSS z) filters. We derive distances for 84 of these galaxies using the method of surface brightness fluctuations (SBFs), present the SBF distance catalog, and use this database to examine the three-dimensional distribution of early-type galaxies in the Virgo Cluster. The SBF distance moduli have a mean (random) measurement error of 0.07 mag (0.5 Mpc), or roughly 3 times better than previous SBF measurements for Virgo Cluster galaxies. Five galaxies lie at a distance of $d \approx 23$ Mpc and are members of the W' cloud. The remaining 79 galaxies have a narrow distribution around our adopted distance of $\langle d \rangle = 16.5 \pm 0.1$ (random mean error) ± 1.1 Mpc (systematic). The rms distance scatter of this sample is $\sigma(d) = 0.6 \pm 0.1$ Mpc, with little or no dependence on morphological type or luminosity class (i.e., 0.7 ± 0.1 and 0.5 ± 0.1 Mpc for the giants and dwarfs, respectively). The back-to-front depth of the cluster measured from our sample of early-type galaxies is 2.4 ± 0.4 Mpc (i.e., $\pm 2\,\sigma$ of the intrinsic distance distribution). The M87 (cluster A) and M49 (cluster B) subclusters are found to lie at distances of 16.7 ± 0.2 and 16.4 ± 0.2 Mpc, respectively. There may be a third subcluster associated with M86. A weak correlation between velocity and line-of-sight distance may be a faint echo of the cluster velocity distribution not having yet completely virialized. In three dimensions, Virgo's early-type galaxies appear to define a slightly triaxial distribution, with axis ratios of (1 : 0.7 : 0.5). The principal axis of the best-fit ellipsoid is inclined $\sim 20°-40°$ from the line of sight, while the galaxies belonging to the W' cloud lie on an axis inclined by $\sim 10°-15°$.

Subject headings: galaxies: clusters: individual (Virgo) — galaxies: distances and redshifts — galaxies: dwarf — galaxies: elliptical and lenticular, cD

1. INTRODUCTION

Currently favored models of structure formation predict that rich clusters are assembled through the accretion, along predominantly radial filaments, of galaxies and subclusters (e.g., van Haarlem & van de Weygaert 1993; Bond et al. 1996; Springel et al. 2005). The presence of distinct substructures in many clusters—identified primarily through statistical analyses of the positions and line-of-sight velocities of individual galaxies, or from an analysis of the cluster X-ray morphology—strongly supports this picture (e.g., Geller & Beers 1982; Dressler & Shectman 1988; Bird 1994; West et al. 1995; Oegerle & Hill 2001) and shows that, even in nearest clusters, the process of virialization is often incomplete (Fitchett & Webster 1987; Merritt 1987; Mellier et al. 1988; Mohr et al. 1993). In principle, accurate distances for individual members of nearby clusters could be used to map out their three-dimensional structure, identify substructures, help disentangle their internal dynamics, and shed light on the processes by which

clusters grow and virialize. In practice, however, the extreme difficulty of measuring distances with the accuracy needed to resolve the cluster along the line of sight ($\sigma_d \lesssim 1$ Mpc) has thwarted such efforts in even the nearest clusters.

At a distance of $\approx$16.5 Mpc, Virgo is the rich cluster nearest to the Milky Way. As such, it offers the best hope to resolve the three-dimensional structure of a rich cluster through distance measurements of individual galaxies. It has long been recognized from the spatial distribution and radial velocities of Virgo galaxies that the cluster has a complex distribution with several distinct components. De Vaucouleurs (1961) first proposed the existence of different substructures—which he termed "clouds"—extending far from the main core. Many subsequent studies helped to characterize the internal structure of the cluster and the relationship with its large-scale surroundings (e.g., de Vaucouleurs & de Vaucouleurs 1973; Helou et al. 1979; Tully & Shaya 1984; Huchra 1985; Tanaka 1985).

To a large extent, the current picture of Virgo's global structure can be traced to the wide-field, photographic imaging survey of Binggeli and collaborators (e.g., Binggeli et al. 1985, 1987, 1993). Galaxy velocities discussed in those papers were collected from previous work (see references in Table IIa in Binggeli et al. 1985 and § 2 in Binggeli et al. 1993). At least six distinct components were adopted in this series of papers: the main body of the cluster (cluster A), which is centered on the cD galaxy M87 (=NGC 4486 = VCC 1316), a smaller subcluster (cluster B) centered on M49 (=NGC 4472 = VCC 1226), three compact clouds offset by $\approx$5° from the main body of the cluster—previously named the M, W, and W' clouds by de Vaucouleurs (1961)—and an elongated Southern Extension cloud that is visible at declinations of $\delta \lesssim 5°$. The center of the Virgo Cluster as a whole—as defined by either the galaxies (Binggeli 1999) or the X-ray-emitting

[2] Department of Physics and Astronomy, Johns Hopkins University, Baltimore, MD; smei@pha.jhu.edu.
[3] GEPI, Observatoire de Paris, Section de Meudon, Meudon Cedex, France.
[4] University of Paris 7 Denis Didevot, Paris Cedex 05, France.
[5] Department of Physics and Astronomy, Washington State University, Pullman, WA.
[6] Herzberg Institute of Astrophysics, National Research Council, Victoria, BC, Canada.
[7] Institute of Astronomy, University of Hawaii, Honolulu, HI.
[8] Gemini Observatory, La Serena, Chile.
[9] Department of Physics and Astronomy, University of Hawaii, Hilo, HI.
[10] European Southern Observatory, Garching, Germany.
[11] Department of Physics, Rochester Institute of Rochester, NY 14623.

gas (Böhringer et al. 1994)—lies close to M87, but is displaced slightly toward M86 (=NGC 4406 = VCC 881). Schindler et al. (1999) have concluded from an optical/X-ray analysis of the cluster that M86 may, like M87 and M49, define the center of its own distinct subcluster (see also Binggeli 1999).

Most of these studies relied on positions and radial velocities of individual galaxies to explore the global structure of the cluster. Clearly, accurate distances for individual galaxies prove invaluable in mapping out the cluster structure. Because of its prime importance in establishing the extragalactic distance scale, searches for Cepheids were carried out successfully in several spiral galaxies belonging to the Virgo Cluster, using both ground-based telescopes and the postrefurbishment *Hubble Space Telescope* (*HST*; Pierce et al. 1994; Freedman et al. 1994; Saha et al. 1994, 1996, 1997; Ferrarese et al. 1996; Gibson et al. 1999; Graham et al. 1999; Macri et al. 1999), while other studies employed a variety of distance indicators to explore the distribution of galaxies within this complex structure. Pierce & Tully (1988) measured Tully-Fisher distances and found evidence for an infall of cluster B onto cluster A, as well as for a significant depth along the line of sight. A significant depth was also suggested by the Tully-Fisher observations of Fukugita et al. (1993). Yasuda et al. (1997) and Federspiel et al. (1998) determined that the W and M clouds are more distant than the bulk of the Virgo galaxies. Gavazzi et al. (1999), using a sample of fundamental plane distances for 59 early-type galaxies and Tully-Fisher distances for 75 late-type galaxies, presented an updated cloud denomination. They argued that cluster B is infalling on cluster A at about 750 km s^{-1} at a relative distance of 1.0 ± 0.1 mag, and placed the W and M clouds at ∼twice the distance of cluster A. They also proposed a new subclassification for cluster A, dividing this structure into four regions: A, corresponding to M87 and the original cluster A; northwest (N); east (E); and south (S). Fouqué et al. (2001) and Solanes et al. (2002) studied the distribution of H i deficient galaxies in these regions.

Unfortunately, with typical errors of ≈0.3 mag (TF) and 0.45 mag (FP), the fundamental plane and Tully-Fisher distance indicators do not have the accuracy needed to resolve structure in the inner regions of the cluster (see Yasuda et al. 1997; Gavazzi et al. 1999). For instance, if the cluster is approximately spherical in shape, then the rms scatter of early-type member galaxies on the plane of the sky translates into an rms depth along the line of sight of ∼0.1 mag. Thus, to fully resolve the structure of the cluster—including the core region, which is dominated by early-type dwarf galaxies (Binggeli et al. 1987)—distances with an accuracy of ≲0.1 mag are required. The method of surface brightness fluctuations (SBFs) offers an attractive route forward, since it is possible to measure distances of this accuracy for a large number of early-type galaxies in a relatively modest allocation of observing time.

The method itself was devised by Tonry & Schneider (1988) and is based on the fact that the Poissonian distribution of unresolved stars in a galaxy produces fluctuations in each pixel of the galaxy image. Since its introduction, the method has been employed by many groups to measure distances for early-type galaxies in the Virgo Cluster, using data from both ground-based telescopes (Tonry et al. 1990, 2000, 2001; Pahre & Mould 1994; Jensen et al. 1998; Jerjen et al. 2004) and from *HST* (Ajhar et al. 1997; Neilsen & Tsvetanov 2000; Jensen et al. 2003). These data have yielded some important insights into the three-dimensional structure of the cluster.

West & Blakeslee (2000) used the SBF catalog of Tonry et al. (2001) to investigate the cluster's *principal axis* and its relation to the surrounding large-scale structure. They found that the brightest ellipticals lie on an axis, inclined ∼$10°$–$15°$ from the line of sight.

More recently, Jerjen et al. (2004) measured SBF distances for 16 Virgo dwarf galaxies, calibrated with stellar population model predictions, and found distances ranging between 14.9 and 21.3 Mpc. They identified two clumps of galaxies, associated with M87 and M86, and determined a back-to-front cluster depth of 6 Mpc (i.e., 2 σ of their galaxy distance moduli distribution). This work effectively ruled out an earlier conclusion by Young & Currie (1995) that the depth of the Virgo early-type dwarfs was about twice as large. Our recent distance measurements based on the half-light radii of globular clusters also argue against such an extremely elongated distribution (see Jordán et al. 2005a).

In this paper we present SBF distance measurements for galaxies in the ACS Virgo Cluster Survey (ACSVCS; Coté et al. 2004, hereafter Paper I). This large *HST* program was designed, in part, to yield homogeneous SBF distances of the highest possible precision for a large sample of early-type galaxies in the Virgo Cluster. We combine our SBF distances with updated radial velocity measurements from the literature to examine the depth and three-dimensional structure of the cluster. Previous papers in this series have discussed the data reduction pipeline (Jordán et al. 2004a, hereafter Paper II), the connection between low-mass X-ray binaries in M87 (Jordán et al. 2004b [Paper III]), the measurement and calibration of surface brightness fluctuation magnitudes (Mei et al. 2005a, 2005b, hereafter Papers IV and V), the morphology, isophotal parameters and surface brightness profiles for early-type galaxies (Ferrarese et al. 2006a [Paper VI]), the connection between globular clusters and ultracompact dwarf galaxies (Haşegan et al. 2005 [Paper VII]), the nuclei of early-type galaxies (Côté et al. 2006 [Paper VIII]) the color distributions of globular clusters (Peng et al. 2006a [Paper IX]), the half light radii of globular clusters and their use as a distance indicator (Jordán et al. 2005a [Paper X]), diffuse star clusters in early-type galaxies (Peng et al. 2006b [Paper XI]) and the connection between supermassive black holes and central stellar nuclei in early-type galaxies (Ferrarese et al. 2006b), and the luminosity functions and color-magnitude relations for globular clusters in early-type galaxies (Jordán et al. 2006a, 2006b [Paper XII]; Mieske et al. 2006b [Paper XIV]).

Throughout this paper, we adopt the standard ΛCDM cosmology—$\Omega_m h^2 = 0.127^{+0.007}_{-0.013}$ and $h = 0.73 \pm 0.03$—from Spergel et al. (2006).

2. THE SELECTION OF ACSVCS PROGRAM GALAXIES

Because of its richness and proximity, the Virgo Cluster covers an area of more than 100 deg^2 on the sky. It has a complex and irregular structure, with galaxies of different morphological type showing different spatial and kinematic distributions (e.g., de Vaucouleurs 1961; Sandage & Tammann 1976; Huchra 1985; Binggeli et al. 1987, 1993; Yasuda et al. 1997; Gavazzi et al. 1999; Solanes et al. 2002; Boselli & Gavazzi 2006). Moreover, there is evidence for systematic differences between the spatial distribution and kinematics of early-type dwarf and giant galaxies in the cluster (Binggeli et al. 1987, 1993; Binggeli 1999). As a further complication, the cluster is projected against a number of distinct foreground and background structures, making it difficult to disentangle its structure from that of the surrounding large-scale environment. In this section, we briefly review the global structure of the cluster and its relationship to the adjacent clouds, and describe the selection function of the ACSVCS galaxies that we use to examine the three-dimensional structure of the cluster.

Figure 1 shows the distribution on the sky of galaxies classified as "members" (*left panel*) and "possible members" (*right panel*) of the Virgo Cluster, using classifications from the Virgo Cluster Catalog of Binggeli et al. (1985) and excluding galaxies
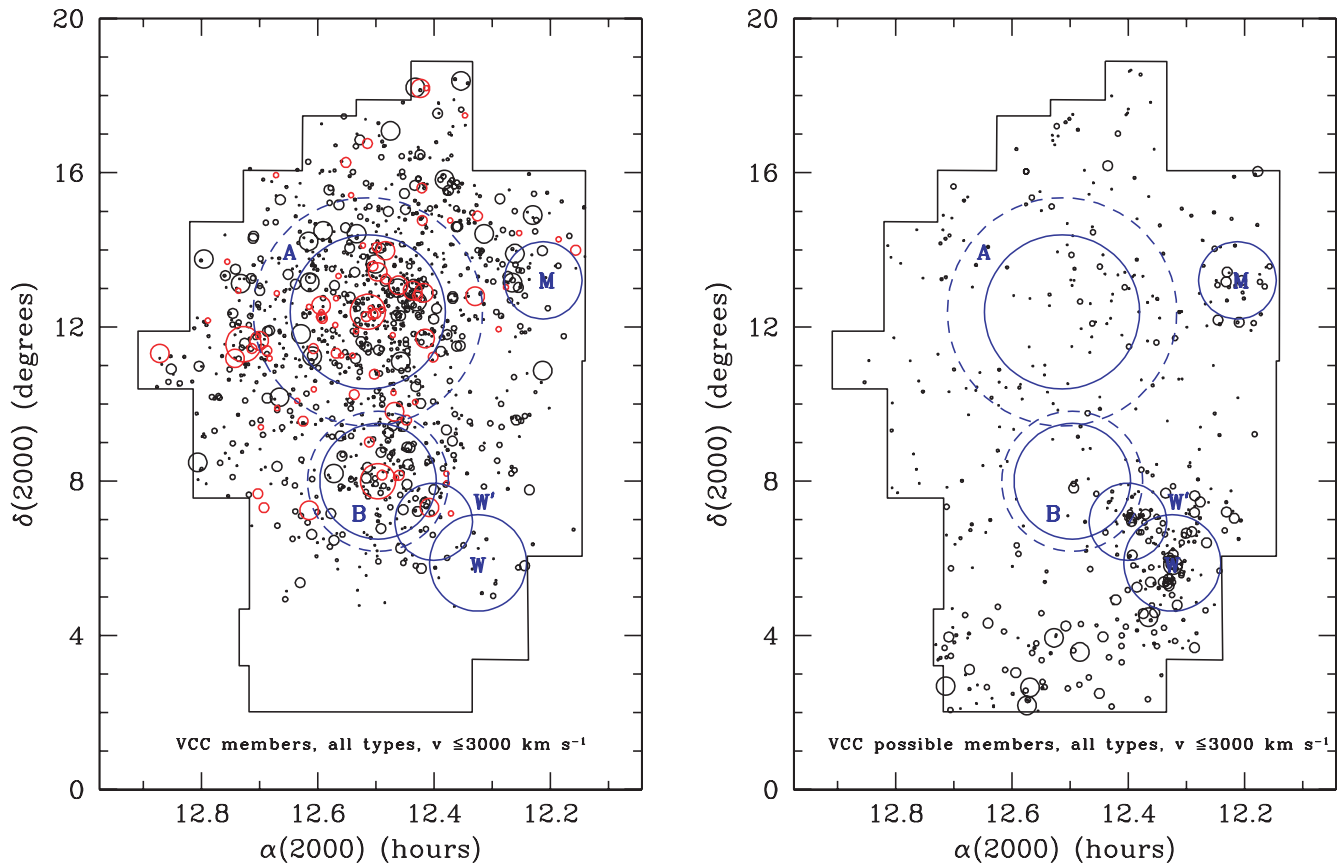
FIG. 1.—*Left:* Tistribution on the sky of galaxies in the Virgo Cluster Catalog (VCC) classified as *members* by Binggeli et al. (1985) and excluding galaxies with heliocentric radial velocities $v_r \geq 3000$ km s^{-1}. A total of 1251 galaxies are plotted, with no restriction on morphological type. Red circles indicate the 100 early-type galaxies from the ACSVCS. In all cases, symbol size is proportional to blue luminosity. The solid blue circles show the location and boundaries of the M87 (A) and M49 (B) clusters—and the M, W', and W clouds—as defined in Binggeli et al. (1987). The larger dashed blue circles centered on M87 and M49 show $r_{200}/2$ for clusters A and B, determined from the optical/X-ray mass models from McLaughlin (1999) and Côté et al. (2001, 2003). The solid lines show the boundaries of the VCC survey, as given in Binggeli et al. (1987). *Right:* VCC galaxies classified as *possible members* by Binggeli et al. (1985) and having heliocentric radial velocities of $v_r \leq 3000$ km s^{-1} for a total of 511 galaxies.

with heliocentric radial velocities[12] of $v_r \geq 3000$ km s^{-1}. In both panels, the symbol size is proportional to blue luminosity. The continuous blue circles identify clusters A and B and clouds M, W, and W' as defined in Binggeli et al. (1987). For comparison, the broken blue circles show the $r_{200}/2$ for clusters A and B, as determined from modeling of X-ray mass profiles of M87/cluster A and M49/cluster B from *ROSAT* (*Röntgensatellit*), optical surface brightness, and integrated-light velocity dispersion profiles for M49 and M87 (McLaughlin 1999; Côté et al. 2001, 2003). These two "subclusters" are evident in the right panel of Figure 1. Note the dominance of cluster A relative to cluster B (e.g., Schindler et al. 1999). The M, W, and W' clouds are apparent in the left panel of Figure 1. The first two of these clouds are thought to lie "at roughly twice the distance of the Virgo Cluster" (Binggeli et al. 1993), while the W' structure is believed to connect cluster B with the W cloud. Further to the south, at declinations of $\delta \lesssim 5°$, the Southern Extension of Virgo defines a filamentary "spur" that may extend toward the background (e.g., Tully 1982; Hoffman et al. 1995).

The red circles in the left panel of Figure 1 show the 100 early-type galaxies from the ACSVCS. As described in Paper I, these

galaxies were drawn from the sample of 163 VCC member galaxies (confirmed by radial velocity measurements) that have blue magnitudes brighter than $B_T = 16$ and with early-type morphological classifications (E, S0, dE, dE,N, dS0, or dS0,N). A total of 63 of these galaxies were excluded from the ACSVCS sample either because they were included in previous *HST* (WFPC2) programs, or because of the lack of a clearly visible bulge component, the presence of strong dust lanes, or signs of strong tidal interactions. The final sample of 100 galaxies includes no objects with declinations $\delta < 7°$, to avoid contamination from the Southern Extension. As Figure 1 shows, most members of the M, W, and W' clouds are classified as *possible* members of Virgo, so our sample should be relatively free from contamination by these structures. However, denominations based on velocity or surface brightness are really "best guesses" (Binggeli et al. 1993) and it is likely that some interlopers from these clouds will appear in our sample. As we will show below, the SBF distances indicate that five galaxies originally classified as members of cluster B are almost certainly associated with the W' cloud.

Radial velocity histograms for the ACSVCS sample (subdivided into giants and dwarfs) are compared to those from the VCC in Figure 2. There is good agreement between the ASCVCS and VCC samples, and we conclude from Figures 1 and 2 that the ACSVCS sample should be a reliable tracer population for the early-type galaxies in the main body of the Virgo Cluster. At the same time, however, Figure 3 serves as a clear reminder that the cluster

---

[12] Based on radial velocity measurements for VCC galaxies compiled from the NASA Extragalactic Database as of May 2006, and including new spectroscopic measurements from the fourth and earlier data releases of the Sloan Digital Sky Survey.
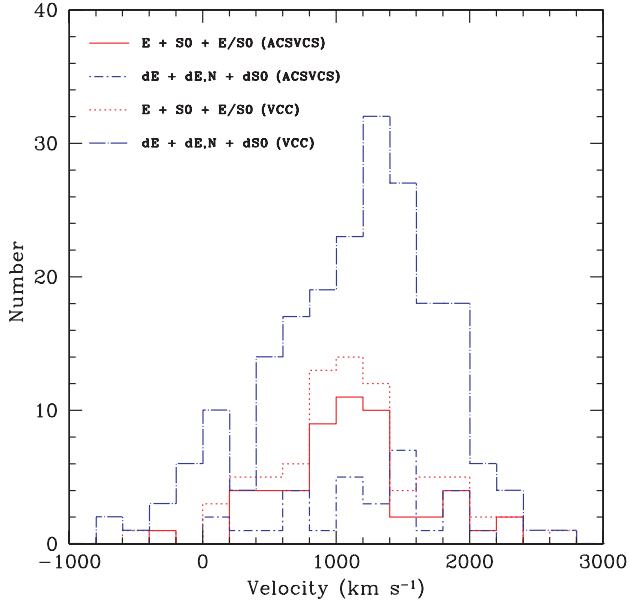
FIG. 2.—Velocity distributions for giant and dwarf galaxies from the Virgo Cluster Catalog (VCC) compared with those from the ACSVCS.

shows unmistakable evidence for a morphology-density relation, with the late-type systems being much less centrally concentrated than the early-type galaxies studied here (Binggeli et al. 1987).

Finding charts for the 100 ACSVCS program galaxies are presented in Figure 4. As we explain below, for 16 of the galaxies in

the survey, it was not possible to derive a reliable SBF distance. These galaxies are highlighted with crosses in Figure 4.

3. SBF DISTANCE MEASUREMENTS

The ACSVCS data reduction and SBF measurement procedures have been fully described in Papers II, IV, and V. In this section, we briefly summarize the main steps involved in the determination of SBF distances.

3.1. *SBF Magnitudes*

The SBF method was introduced by Tonry & Schneider (1988; for reviews see Jacoby et al. 1992 and Blakeslee et al. 1999). The SBF are defined as the variance of the normalized Poissonian fluctuations of the galaxy stellar population. The variance is normalized by the galaxy surface brightness, then converted to a magnitude, called $\overline{m}$. The measured $\overline{m}$ depends on galaxy distance, and varies as a function of the stellar population age and metallicity. To obtain distance measurements, SBF magnitudes must therefore be carefully calibrated in terms of stellar population observables— usually galaxy colors. Tonry et al. (1997, 2001) have shown that I-band SBF magnitudes in elliptical galaxies can be calibrated as a function of the $(V - I)$ galaxy color over the range $1 < (V - I)_0 < 1.3$ mag, with an internal scatter $\lesssim 0.1$ mag. This general approach has been used in many programs to measure early-type galaxy distances with both ground-based telescopes and *HST* (Ajhar et al. 1997, 2001; Tonry et al. 1997, 2001; Jensen et al. 1999, 2003; Blakeslee et al. 2001, 2002; Mei et al. 2001, 2003; Liu & Graham 2001; Liu et al. 2002; Mieske et al. 2003; Cantiello et al. 2005; and references in Paper IV).
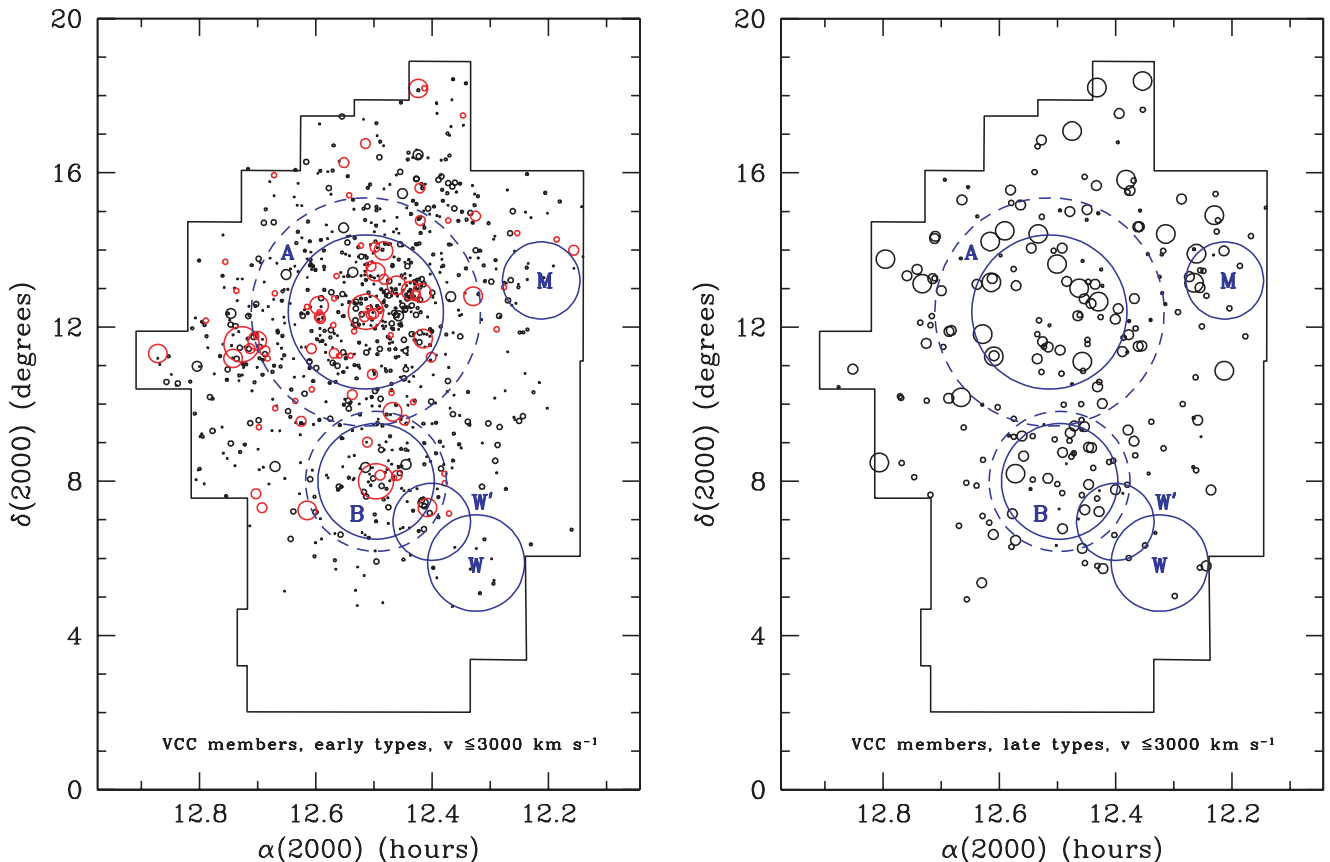
FIG. 3.—The distribution on the sky of *member* galaxies from the Virgo Cluster Catalog (VCC) divided on the basis of morphology. *Left:* 938 galaxies with *early-type* morphologies (i.e., E, S0, dE, dE,N, dS0, or dS0,N) and having $v_r \leq 3000$ km s^{-1}. Red symbols show the 100 early-type galaxies from the ACSVCS. *Right:* Same as the previous panel, except for 225 member galaxies with $v_r \leq 3000$ km s^{-1} and *late-type* morphologies.
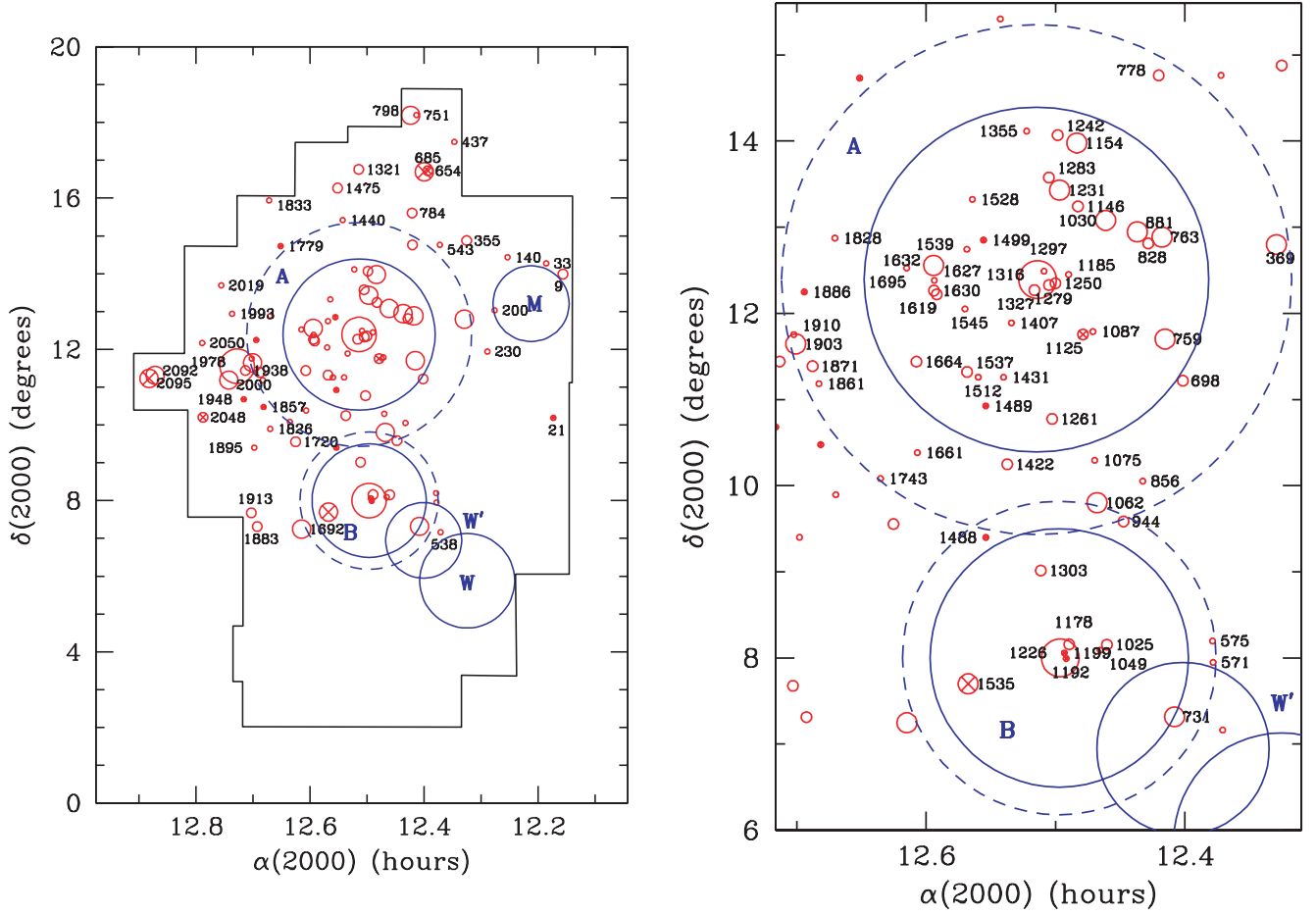
Fig. 4.— Distribution of galaxies from the ACSVCS. *Left:* Finding charts for galaxies beyond $r_{200}/2$ for clusters A and B (centered on M87 and M49, respectively). Circles with crosses show galaxies for which it was not possible to measure a reliable SBF distance. *Right:* A magnified view of the regions centered on M87 and M49, with the remaining galaxies from the ACSVCS labeled. Circles with crosses show those galaxies for which it was not possible to measure a reliable SBF distance.

Each of the 100 ACSVCS galaxies was observed for a single orbit with *HST*, for a total of 750 s in F475 (g_{475}) and 1210 s in F850LP (z_{850}). The choice of the g_{475} and z_{850} bandpasses was dictated by their high throughput and sensitivity to changes in stellar population age and metallicity. Our SBF measurements were performed in the z_{850} filter and calibrated in terms of the ($g_{475} - z_{850}$)$_0$ galaxy color. As shown in Figure 7 of Paper I, which is based on model predictions from Blakeslee et al. (2001), SBF measurements in this filter will be brighter, and show less scatter, than corresponding measurements made in the *V*, *R* or *I*-filters. Our data reduction procedures account for the significant geometrical distortions caused by the off-axis location of the ACS/WFC in the *HST* focal plane and were optimized to guard against possible biases introduced by resampling the pixel values (see Papers II and IV).

3.2. *Choice of Distance Calibration*

Details on the ACSVCS SBF calibration are given in Paper V, which presents a broken linear calibration for the absolute SBF magnitude $\overline{M}_{850}$:

$$\overline{M}_{850} = \begin{cases} -2.06 \pm 0.04 + (0.9 \pm 0.2)[(g_{475} - z_{850})_0 - 1.3], \\ \quad \text{if } 1.0 \leq (g_{475} - z_{850})_0 \leq 1.3, \\ -2.06 \pm 0.04 + (2.0 \pm 0.2)[(g_{475} - z_{850})_0 - 1.3], \\ \quad \text{if } 1.3 < (g_{475} - z_{850})_0 \leq 1.6, \end{cases}$$

(1)

These color regimes correspond roughly to different morphological types, with early-type giants at the red end, and early-type dwarfs at the blue. This division is evident in the color-magnitude diagram shown in the top panel of Figure 5. Different symbols correspond to the dwarfs (*blue triangles*) and giants (*red circles*) in the ACSVCS sample, based on the VCC morphologies given in Binggeli et al. (1985). While a color of ($g_{475} - z_{850}$)$_0 = 1.3$ serves to roughly divide the sample into dwarfs and giants, we caution that this division is not unique. In any case, the bottom panel of Figure 5 plots apparent SBF magnitude against galaxy color, showing that there are no systematic differences in the results for red or blue galaxies. The long-dashed curve shows the calibration given by equation (1). The two other curves show alternate choices for the SBF calibration; these alternate relations are discussed in the Appendix, along with a discussion of the possible biases and errors that may arise from our choice of calibration.

The absolute zero point in equation (1) was derived from the Tonry et al. (2001) Virgo distance modulus, corrected by the Udalski et al. (1999) Cepheid period-luminosity relation adopted for the H_0 Key Project distances (Freedman et al. 2001), which gives 31.09 ± 0.03 mag (see the discussion in Paper V). The zero-point uncertainty includes all sources of internal error; there is an additional systematic uncertainty of ~ 0.15 mag, due to the uncertainty of Cepheid distance measurements in the distance scale calibration. Comparing to stellar population models of Bruzual & Charlot (2003), our results are consistent with model predictions in the range $1.3 < (g_{475} - z_{850})_0 \leq 1.6$ mag. In the range
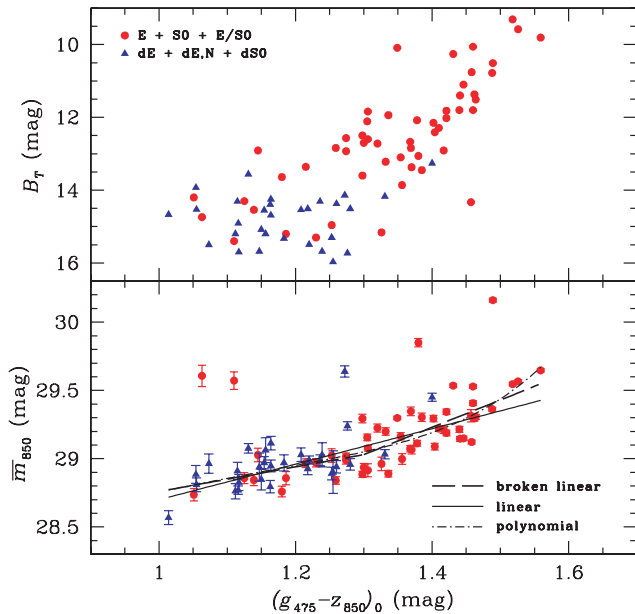
Fig. 5.—*Top:* Color magnitude diagram in the B_T-$(g_{475} - z_{850})_0$ plane for 84 galaxies from the ACSVCS with measured SBF magnitudes (see Table 1). Galaxies with giant and dwarf classifications from Binggeli et al. (1985) are plotted as red circles and blue triangles, respectively. *Bottom:* SBF magnitude, $\overline{m}_{850}$, as a function of galaxy color for the 84 galaxies shown in the top panel. Three different SBF measurement calibrations are overlaid: (1) a broken linear relation matched at a color of $(g_{475} - z_{850})_0 = 1.3$ mag (*heavy dashed line*; eq. (1); (2) a single linear relation (*solid line*; eq. [A1]); and (3) a fourth-order polynomial fit (eq. [A2], *dashed-dotted curve*). Galaxies with giant and dwarf classifications from Binggeli et al. (1985) are plotted as red circles and blue triangles, respectively. Five galaxies belonging to the W' cloud lie ~0.7 mag above the fitted relations.

$0.9 \le (g_{475} - z_{850})_0 \le 1.3$ mag, the empirical slope is somewhat steeper than the Bruzual & Charlot model predictions. However, as discussed by Mieske et al. (2006a), other models (Blakeslee et al. 2001; Cantiello et al. 2003) predict somewhat steeper SBF-color relations in the blue, more in line with the empirical behavior.

Using the above calibration, we derived galaxy distances for 84 galaxies in our sample. Distances were not measured for seven galaxies with very blue colors of $(g_{475} - z_{850})_0 \le 1$. In fact, the standard deviation of SBF magnitudes increases as the $(g_{475} - z_{850})_0$ color decreases, making it difficult to establish a reliable calibration for these blue colors (see the discussion in Paper V). Nine other galaxies were not included in the sample because of difficult sky subtraction, or because they are edge-on disk or barred galaxies, which are especially challenging for SBF measurements.

3.3. *SBF Distance Catalog*

The final SBF measurements and distance moduli from the ACSVCS are presented in Table 1. The columns of this table record the following: (1) ID number from Coté et al. (2004); (2) VCC number from Binggeli et al. (1985); (3) galaxy $(g_{475} - z_{850})_0$ color over the same range of annuli used for the SBF measurements (see Paper V); (4) SBF magnitude $\overline{M}_{850}$; (5) distance modulus obtained using the broken linear calibration (eq. [1]); (6) blue magnitude, B_T, from Binggeli et al. (1985); (7) heliocentric radial velocity from Huchra (1985) and Binggeli et al. (1993); (8) morphological type from Binggeli et al. (1985); (9) identification numbers from the Messier, NGC, IC, and UGC catalogs; and (10) numerical code to identify those galaxies without measured SBF magnitudes or distances, or galaxies with uncertain measurements.

As in Paper I, the identification numbers in column (1) run from the brightest to the faintest apparent blue magnitudes. In the

Appendix, we report distances for these same galaxies obtained with the alternate calibrations.

3.4. *Comparison with Previous SBF Surveys*

Table 2 and Figure 6 compare our distances with those reported in three previous SBF surveys of the Virgo cluster: Neilsen & Tsvetanov (2000), Tonry et al. (2001), and Jerjen et al. (2004). Note that the Tonry et al. (2001) measurements were recalibrated to the same zero point that we use in this work, and that no zero-point corrections have been applied to either the Neilsen & Tsvetanov (2000) or Jerjen et al. (2004) data sets.

Neilsen & Tsvetanov (2000) measured SBF distances for 15 bright early-type Virgo cluster galaxies using *HST* WFPC2 images in the F814W bandpass calibrated against the stellar population models of G. Worthey et al. (1998, private communication). These models gave reasonable agreement with the ground-based calibration of Tonry et al. (1997). The 15 galaxies from Neilsen & Tsvetanov (2000) are also included in the ACSVCS; the top panel of Figure 6 compares the measured distance moduli for these objects. The dashed line shows the best-fit linear relation, accounting for the uncertainties in both measurements (Press et al. 1992). The slope of this relation is 1.03 ± 0.18, with an rms scatter of 0.26 mag.

The survey of Tonry et al. (2001) is the largest SBF survey currently available, consisting of SBF measurements for 300 galaxies out to $cz \sim 4000$ km s^{-1}. Tonry et al. (2001) measured and calibrated *I*-band SBF as a function of $(V - I)$ color. A total of 26 galaxies in our sample have distance measurements from this survey. The average uncertainty in the Tonry et al. (2001) distance moduli is 0.20 mag for these galaxies (with a median of 0.16 mag), roughly 3 times larger than the average (and median) ACSVCS uncertainty of 0.07 mag. The measurements are compared in the middle panel of Figure 6. The dashed line shows the best-fit linear relation, which has a slope of 0.99 ± 0.16 and an rms scatter of 0.22 mag.

The Jerjen et al. (2004) sample consists of 16 dwarf galaxies, of which six are in common with our survey. Their work made use of deep *R* and *B*-band imaging with FORS1 on the Very Large Telescope (VLT). Distances were derived by calibrating the *R*-band SBF measurements as a function of $(B - R)$ color, using stellar population models from Worthey (1994) (as described in Jerjen et al. 2001). For two galaxies in common with our survey, Jerjen et al. (2004) list two values for the distance modulus, depending on their choice of calibration. Note that stellar population models make widely varying SBF predictions at the blue colors of these dwarfs (e.g., Mieske et al. 2006a). Given the relatively small sample of galaxies in common between the two studies, and the fact that all six galaxies are located close to the mean cluster distance, we do not attempt a regression analysis. The rms scatter about the one-to-one relation shown in the bottom panel of Figure 6 is 0.32 mag; however, removing the one large outlier (VCC 1422) reduces the scatter to 0.18 mag.

We conclude from Table 2 and Figure 6 that there is good agreement between our distance moduli and those from previous studies. At the same time, our new SBF distances have a mean precision that is 3–4 times better than the previous measurements, and our sample of 84 galaxies with measured SBF distances represents more than a three-fold increase over any single previous SBF survey in Virgo.

4. RESULTS

4.1. *Cluster Structure and Line-of-Sight Depth*

Figures 7 and 8 illustrate the spatial and kinematic structure of the cluster along the line of sight, using the SBF distances listed

TABLE 1
S$_{\text{BF}}$ D$_{\text{ISTANCES FOR}}$ ACSVCS G$_{\text{ALAXIES}}$

ID No. (1)	VCC No. (2)	$(g_{475} - z_{850})_0$ (mag) (3)	$\overline{M}_{850}$ (mag) (4)	$(m - M)$ (mag) (5)	B_T^b (mag) (6)	$\langle v_r \rangle$ (km s^{-1}) (7)	Type (8)	Other (9)	Notes (10)
1	1226	1.52 ± 0.01	29.55 ± 0.01	31.17 ± 0.07	9.31	997 ± 7	E2/S0$_1$(2)	M49, N4472	
2	1316	1.53 ± 0.01	29.57 ± 0.01	31.18 ± 0.07	9.58	1307 ± 7	E0	M87, N4486	
3	1978	1.56 ± 0.01	29.65 ± 0.01	31.19 ± 0.07	9.81	1117 ± 6	S0$_1$(2)	M60, N4649	
4	881	1.46 ± 0.01	29.53 ± 0.04	31.13 ± 0.07	10.06	−244 ± 5	S0$_1$(3)/E3	M86, N4406	
5	798	1.35 ± 0.01	29.30 ± 0.01	31.26 ± 0.05	10.09	729 ± 2	S0$_1$(3) pec	M85, N4382	
6	763	1.43 ± 0.01	29.54 ± 0.02	31.33 ± 0.05	10.26	1060 ± 6	E1	M84, N4374	
7	731	1.49 ± 0.01	30.16 ± 0.02	31.84 ± 0.06	10.51	1243 ± 6	E3	N4365	
8	1535	. . .	. . .	. . .	10.61	448 ± 8	S0$_3$(6)	N4526	1
9	1903	1.46 ± 0.01	29.12 ± 0.01	30.87 ± 0.06	10.76	410 ± 6	E4	M59, N4621	
10	1632	1.49 ± 0.01	29.19 ± 0.02	31.00 ± 0.06	10.78	340 ± 4	S0$_1$(0)	M89, N4552	
11	1231	1.45 ± 0.01	29.15 ± 0.02	30.92 ± 0.06	11.10	2244 ± 2	E5	N4473	
12	2095	. . .	. . .	. . .	11.18	984 ± 11	S0$_1$(9)	N4762	2
13	1154	1.46 ± 0.01	29.29 ± 0.02	31.03 ± 0.06	11.37	1210 ± 16	S0$_3$(2)	N4459	
14	1062	1.44 ± 0.01	29.15 ± 0.02	30.92 ± 0.06	11.40	532 ± 8	SB0$_1$(6)	N4442	
15	2092	1.46 ± 0.01	29.31 ± 0.02	31.04 ± 0.06	11.51	1347 ± 9	SB0$_1$(5)	N4754	
16	369	1.44 ± 0.01	29.22 ± 0.02	31.00 ± 0.06	11.80	1009 ± 13	SB0$_1$	N4267	
17	759	1.46 ± 0.01	29.41 ± 0.02	31.15 ± 0.06	11.80	943 ± 19	SB0$_2$(r)(3)	N4371	
18	1692	1.42 ± 0.01	29.34 ± 0.02	31.16 ± 0.06	11.82	1730 ± 13	S0$_1$(7)/E7	N4570	
19	1030	1.31 ± 0.01	29.08 ± 0.02	31.12 ± 0.05	11.84	801 ± 10	SB0$_1$(6)	N4435	
20	2000	1.34 ± 0.01	28.89 ± 0.02	30.88 ± 0.05	11.94	1083 ± 4	E3/S0$_1$(3)	N4660	
21	685	. . .	. . .	. . .	11.99	1200 ± 15	S0$_1$(8)	N4350	1, 2
22	1664	1.42 ± 0.01	29.19 ± 0.02	31.00 ± 0.06	12.02	1142 ± 2	E6	N4564	
23	654	. . .	. . .	. . .	12.03	950 ± 9	RSB0$_2$(5)	N4340	2
24	944	1.38 ± 0.01	29.11 ± 0.02	31.02 ± 0.06	12.08	820 ± 12	S0$_1$(7)	N4417	
25	1938	1.30 ± 0.01	29.16 ± 0.02	31.21 ± 0.05	12.11	1164 ± 10	S0$_1$(7)	N4638	
26	1279	1.40 ± 0.01	29.29 ± 0.02	31.15 ± 0.06	12.15	1349 ± 3	E2	N4478	
27	1720	1.41 ± 0.01	29.22 ± 0.02	31.06 ± 0.06	12.29	2273 ± 12	S0$_{1/2}$(4)	N4578	5
28	355	1.40 ± 0.01	29.09 ± 0.02	30.94 ± 0.06	12.41	1359 ± 4	SB0$_{2/3}$	N4262	
29	1619	1.30 ± 0.01	28.89 ± 0.02	30.95 ± 0.05	12.50	381 ± 9	E7/S0$_1$(7)	N4550	
30	1883	1.28 ± 0.01	29.02 ± 0.02	31.10 ± 0.05	12.57	1875 ± 22	RSB0$_{1/2}$	N4612	
31	1242	1.31 ± 0.01	28.92 ± 0.05	30.96 ± 0.07	12.60	1588 ± 7	S0$_1$(8)	N4474	
32	784	1.37 ± 0.01	29.07 ± 0.02	31.00 ± 0.06	12.67	1069 ± 10	S0$_1$(2)	N4379	
33	1537	1.30 ± 0.01	28.94 ± 0.03	31.00 ± 0.05	12.70	1342 ± 8	SB0$_2$(5)	N4528	
34	778	1.32 ± 0.01	29.22 ± 0.03	31.25 ± 0.06	12.72	1375 ± 11	S0$_1$(3)	N4377	
35	1321	1.26 ± 0.01	28.84 ± 0.03	30.94 ± 0.05	12.84	967 ± 6	S0$_1$(1)	N4489	
36	828	1.37 ± 0.01	29.35 ± 0.03	31.27 ± 0.06	12.84	472 ± 11	E5	N4387	
37	1250	1.14 ± 0.01	29.03 ± 0.05	31.23 ± 0.07	12.91	1970 ± 11	S0$_3$(5)	N4476	
38	1630	1.42 ± 0.01	29.21 ± 0.03	31.04 ± 0.06	12.91	1172 ± 6	E2	N4551	
39	1146	1.27 ± 0.01	28.99 ± 0.03	31.07 ± 0.05	12.93	635 ± 6	E1	N4458	
40	1025	1.38 ± 0.02	29.85 ± 0.03	31.75 ± 0.06	13.06	1071 ± 6	E0/S0$_1$(0)	N4434	5
41	1303	1.35 ± 0.01	29.16 ± 0.03	31.12 ± 0.06	13.10	875 ± 10	SB0$_1$(5)	N4483	
42	1913	1.33 ± 0.01	29.20 ± 0.03	31.20 ± 0.06	13.22	1892 ± 37	E7	N4623	
43	1327	1.40 ± 0.01	29.45 ± 0.03	31.31 ± 0.06	13.26	150 ± 45	E2	N4486A	3
44	1125	. . .	. . .	. . .	13.30	165 ± 6	S0$_1$(9)	N4452	2
45	1475	1.21 ± 0.01	28.97 ± 0.03	31.10 ± 0.06	13.36	951 ± 11	E2	N4515	
46	1178	1.37 ± 0.01	29.07 ± 0.03	31.00 ± 0.06	13.37	1243 ± 2	E3	N4464	
47	1283	1.38 ± 0.01	29.30 ± 0.03	31.20 ± 0.06	13.45	876 ± 10	SB0$_2$(2)	N4479	
48	1261	1.13 ± 0.01	29.08 ± 0.04	31.29 ± 0.06	13.56	1871 ± 16	d:E5,N	N4482	
49	698	1.30 ± 0.01	29.29 ± 0.03	31.36 ± 0.05	13.60	2070 ± 7	S0$_1$(8)	N4352	
50	1422	1.18 ± 0.01	28.76 ± 0.04	30.93 ± 0.06	13.64	1288 ± 10	E1,N:	I3468	
51	2048	. . .	. . .	. . .	13.81	1084 ± 12	d:S0(9)	I3773	2
52	1871	1.36 ± 0.01	29.00 ± 0.04	30.95 ± 0.06	13.86	567 ± 10	E3	I3653	
53	9	1.05 ± 0.01	28.89 ± 0.07	31.17 ± 0.09	13.93	1804 ± 49	dE1,N	I3019	
54	575	1.27 ± 0.01	29.64 ± 0.04	31.72 ± 0.06	14.14	1231 ± 9	E4	N4318	
55	1910	1.33 ± 0.01	29.03 ± 0.03	31.03 ± 0.06	14.17	206 ± 26	dE1,N	I809	
56	1049	1.05 ± 0.01	28.74 ± 0.05	31.02 ± 0.08	14.20	716 ± 36	S0(4)	U7580	
57	856	1.16 ± 0.01	28.95 ± 0.04	31.13 ± 0.07	14.25	1025 ± 10	dE1,N	I3328	
58	140	1.13 ± 0.01	28.86 ± 0.04	31.07 ± 0.07	14.30	1013 ± 26	S0$_{1/2}$(4)	I3065	
59	1355	1.12 ± 0.01	28.91 ± 0.06	31.14 ± 0.08	14.31	1332 ± 63	dE2,N	I3442	
60	1087	1.24 ± 0.01	28.99 ± 0.04	31.11 ± 0.06	14.31	675 ± 12	dE3,N	I3381	
61	1297	1.46 ± 0.01	29.31 ± 0.04	31.06 ± 0.07	14.33	1555 ± 4	E1	N4486B	
62	1861	1.26 ± 0.01	28.94 ± 0.05	31.04 ± 0.06	14.37	629 ± 20	dE0,N	I3652	
63	543	1.16 ± 0.01	28.79 ± 0.05	30.98 ± 0.07	14.39	985 ± 12	dE5	U7436	
64	1431	1.28 ± 0.01	28.96 ± 0.04	31.04 ± 0.06	14.51	1505 ± 21	dE0,N	I3470	

TABLE 1—*Continued*

ID No. (1)	VCC No. (2)	$(g_{475} - z_{850})_0$ (mag) (3)	$\overline{M}_{850}$ (mag) (4)	$(m - M)$ (mag) (5)	B_T^b (mag) (6)	$\langle v_r \rangle$ (km s^{-1}) (7)	Type (8)	Other (9)	Notes (10)
65..........	1528	1.22 ± 0.01	28.93 ± 0.04	31.06 ± 0.06	14.51	1608 ± 35	d:E1	I3501	
66..........	1695	1.05 ± 0.01	28.81 ± 0.05	31.09 ± 0.08	14.53	1547 ± 29	dS0:	I3586	
67..........	1833	1.14 ± 0.01	28.84 ± 0.04	31.05 ± 0.07	14.54	1679 ± 34	S0$_1$(6)		
68..........	437	1.21 ± 0.01	29.03 ± 0.05	31.17 ± 0.07	14.54	1474 ± 46	dE5,N	U7399A	
69..........	2019	1.15 ± 0.01	28.97 ± 0.04	31.16 ± 0.07	14.55	1895 ± 44	dE4,N	I3735	
70..........	33	1.01 ± 0.01	28.57 ± 0.05	30.89 ± 0.09	14.67	1093 ± 52	d:E2,N:	I3032	
71..........	200	1.16 ± 0.01	29.11 ± 0.05	31.30 ± 0.07	14.69	16 ± 20	dE2,N		
72..........	571	1.06 ± 0.01	29.61 ± 0.08	31.88 ± 0.10	14.74	1047 ± 37	SB0$_1$(6)		5 + dust
73..........	21	0.86 ± 0.01	28.97 ± 0.04	...	14.75	486 ± 25	dS0(4)	I3025	6
74..........	1488	0.95 ± 0.01	28.57 ± 0.05	...	14.76	1079 ± 25	E6:	I3487	6
75..........	1779	0.90 ± 0.01	28.42 ± 0.06	...	14.83	1313 ± 45	dS0(6):	I3612	6
76..........	1895	1.12 ± 0.01	28.77 ± 0.03	31.00 ± 0.06	14.91	1032 ± 51	d:E6	U7854	
77..........	1499	0.67 ± 0.01	27.97 ± 0.07	...	14.94	−575 ± 35	E3 pec or S0	I3492	6
78..........	1545	1.25 ± 0.01	29.02 ± 0.05	31.13 ± 0.07	14.96	2000 ± 22	E4	I3509	
79..........	1192	...	...	...	15.04	1423 ± 11	E3	N4467	4
80..........	1857	...	...	...	15.07	634 ± 69	dE4:,N?	I3647	4
81..........	1075	1.15 ± 0.01	28.85 ± 0.08	31.04 ± 0.09	15.08	1844 ± 40	dE4,N	I3383	
82..........	1948	0.99 ± 0.01	28.80 ± 0.10	...	15.10	1672 ± 98	dE3		6
83..........	1627	1.32 ± 0.13	28.96 ± 0.05	30.97 ± 0.27	15.16	236 ± 41	E0		5
84..........	1440	1.19 ± 0.01	28.86 ± 0.05	31.02 ± 0.07	15.20	382 ± 21	E0	I798	
85..........	230	1.16 ± 0.01	29.06 ± 0.09	31.25 ± 0.10	15.20	1429 ± 20	dE4:,N:	I3101	
86..........	2050	1.11 ± 0.01	28.76 ± 0.06	30.99 ± 0.08	15.20	1193 ± 48	dE5:,N	I3779	
87..........	1993	1.23 ± 0.01	28.97 ± 0.03	31.09 ± 0.05	15.30	875 ± 50	E0		
88..........	751	1.25 ± 0.01	28.89 ± 0.05	30.99 ± 0.06	15.30	697 ± 36	dS0	I3292	
89..........	1828	1.18 ± 0.01	28.97 ± 0.06	31.13 ± 0.08	15.33	1569 ± 25	dE2,N	I3635	
90..........	538	1.11 ± 0.01	29.57 ± 0.06	31.80 ± 0.09	15.40	620 ± 37	E0	N4309A	
91..........	1407	1.22 ± 0.01	28.99 ± 0.03	31.12 ± 0.05	15.49	1001 ± 11	dE2,N	I3461	
92..........	1886	0.95 ± 0.01	28.61 ± 0.14	...	15.49	1159 ± 65	dE5,N		6
93..........	1199	...	...	...	15.50	1201 ± 21	E2		4
94..........	1743	1.07 ± 0.01	28.96 ± 0.07	31.23 ± 0.09	15.50	1279 ± 10	dE6	I3602	
95..........	1539	1.15 ± 0.01	28.94 ± 0.10	31.14 ± 0.11	15.68	1491 ± 25	dE0,N		
96..........	1185	1.24 ± 0.01	29.03 ± 0.09	31.14 ± 0.10	15.68	500 ± 50	dE1,N		
97..........	1826	1.12 ± 0.01	28.83 ± 0.06	31.05 ± 0.08	15.70	2033 ± 38	dE2,N	I3633	
98..........	1512	1.28 ± 0.01	29.24 ± 0.03	31.32 ± 0.05	15.73	762 ± 35	dS0 pec		
99..........	1489	0.99 ± 0.01	28.96 ± 0.09	...	15.89	80 ± 50	dE5,N?	I3490	6
100.........	1661	1.26 ± 0.01	28.90 ± 0.16	31.00 ± 0.16	15.97	1457 ± 34	dE0,N		

Notes.—Col. (1): no SBF measurement possible (dust); col. (2): no SBF measurement possible (edge-on disk or bar); col. (3): very uncertain SBF measurement due to the precence of a bright star; col. (4): no SBF measurement possible (sky subtraction); col. (5): uncertain SBF measurement because of difficult sky or galaxy model subtraction; col. (6): no SBF distance (galaxy too blue).

in Table 1. Four "slices" in distance are shown in Figure 7: (1) $14.5 < d \leq 16$ Mpc (*top left*); (2) $16 < d \leq 17.5$ Mpc (*top right*); (3) $17.5 < d \leq 19$ Mpc (*bottom left*); and (4) $d > 19$ Mpc. The first of these panels shows a preponderance of galaxies in the eastern side of the cluster. Most of the galaxies in the sample, which belong to the M87/A subcluster, appear in the second panel (16–17.5 Mpc). Still more distant galaxies (17.5–19 Mpc) appear in the third panel and lie mainly in the western half of the cluster. A separate, more distant group at $d \approx 23$ Mpc (visible in the fourth panel) is almost certainly associated with the W′ cloud, which is centered at $\alpha \approx 12^{\rm h}24^{\rm m}$ and $\delta \approx 7°$ (J2000.0). In Figure 8, four ranges in heliocentric radial velocity are shown: $v_r \leq 450$ km s^{-1} (*top left*); $450 < v_r \leq 1050$ km s^{-1} (*top right*); $1050 < v_r \leq 1650$ km s^{-1} (*bottom left*); and $1650 < v_r \leq 3000$ km s^{-1} (*bottom right*). In the bottom right panel, we notice that all the group of galaxies east (*left in the figure*) of cluster B have $v_r > 1650$ km s^{-1}. Excluding the galaxies with $d \approx 23$ Mpc, Figures 7 and 8 suggest that there is an east-to-west gradient in distance across the face of the cluster, with the eastern portion of the cluster lying slightly in the foreground. We shall return to this issue in § 4.3.

To estimate the line-of-sight depth of the cluster, we begin by dividing the ACSVCS galaxies in various subsamples: i.e., giants versus dwarfs, and red versus blue galaxies. Distance histograms for these subsamples are shown in the top panels of Figure 9. The smooth curves in each panel show Gaussian distributions with the parameters listed in Table 3. For various subsamples, the columns of this table record the number of galaxies in each subsample, N, the mean distance modulus, $\overline{(m - M)}$, the observed dispersion, $\sigma(m - M)_o$, the average uncertainty on the individual distance moduli, $\overline{\sigma(m - M)}_m$, and the *intrinsic* dispersion in distance modulus, $\sigma(m - M)_i$. The final four columns give the mean distance, $\overline{d}$, the intrinsic dispersion in distance, $\sigma(d)$, mean radial velocity, $\overline{v}_r$, and the measured velocity dispersion, σ_{v_r}. We take the intrinsic dispersion in distance modulus for each subsample to be

$$\sigma(m - M)_i = \left[\sigma(m - M)_o^2 - \overline{\sigma(m - M)}_m^2 - \sigma(m - M)_c^2 \right]^{1/2},$$

where $\sigma(m - M)_c = 0.05$ mag is the estimated "cosmic scatter" in the fluctuation magnitude (e.g., Tonry et al. 1997). We see from

TABLE 2
COMPARISON WITH THE PREVIOUS SBF DISTANCE MEASUREMENTS

			$(m - M)$			
ID No.	VCC No.	OTHER NAME	ACSVCS (mag)	NT00[a] (mag)	T01[b] (mag)	J04[c] (mag)
1..............................	1226	NGC 4472	31.17 ± 0.07	30.94 ± 0.09	31.06 ± 0.10	...
2..............................	1316	NGC 4486	31.18 ± 0.07	31.15 ± 0.12	31.03 ± 0.16	...
3..............................	1978	NGC 4649	31.19 ± 0.07	31.06 ± 0.11	31.13 ± 0.15	...
4..............................	881	NGC 4406	31.13 ± 0.07	31.45 ± 0.12	31.17 ± 0.14	...
5..............................	798	NGC 4382	31.26 ± 0.05	...	31.33 ± 0.14	...
6..............................	763	NGC 4374	31.33 ± 0.05	31.17 ± 0.10	31.32 ± 0.11	...
7..............................	731	NGC 4365	31.84 ± 0.06	31.94 ± 0.15	31.55 ± 0.17	...
9..............................	1903	NGC 4621	30.87 ± 0.06	30.82 ± 0.10	31.31 ± 0.20	...
10..............................	1632	NGC 4552	31.00 ± 0.06	31.00 ± 0.10	30.93 ± 0.14	...
11..............................	1231	NGC 4473	30.92 ± 0.06	31.07 ± 0.11	30.98 ± 0.13	...
13..............................	1154	NGC 4459	31.03 ± 0.06	...	31.04 ± 0.22	...
15..............................	2092	NGC 4754	31.04 ± 0.06	...	31.13 ± 0.14	...
20..............................	2000	NGC 4660	30.88 ± 0.05	31.30 ± 0.16	30.54 ± 0.19	...
22..............................	1664	NGC 4564	31.00 ± 0.06	...	30.88 ± 0.17	...
25..............................	1938	NGC 4638	31.21 ± 0.05	...	31.68 ± 0.26	...
26..............................	1279	NGC 4478	31.15 ± 0.06	31.10 ± 0.11	31.29 ± 0.28	...
27..............................	1720	NGC 4578	31.06 ± 0.06	...	31.34 ± 0.13	...
29..............................	1619	NGC 4550	30.95 ± 0.05	30.82 ± 0.22	31.00 ± 0.20	...
32..............................	784	NGC 4379	31.00 ± 0.06	...	30.76 ± 0.41	...
35..............................	1321	NGC 4489	30.94 ± 0.05	...	31.26 ± 0.15	...
36..............................	828	NGC 4387	31.27 ± 0.06	...	31.65 ± 0.73	...
37..............................	1250	NGC 4476	31.23 ± 0.07	31.60 ± 0.16	31.18 ± 0.17	...
38..............................	1630	NGC 4551	31.04 ± 0.06	...	31.19 ± 0.17	...
39..............................	1146	NGC 4458	31.07 ± 0.05	31.78 ± 0.59	31.18 ± 0.12	...
40..............................	1025	NGC 4434	31.75 ± 0.06	...	32.14 ± 0.17	...
48..............................	1261	NGC 4482	31.29 ± 0.06	...	...	31.34 ± 0.16
				...	...	31.74 ± 0.21
50..............................	1422	IC 3468	30.93 ± 0.06	...	...	31.64 ± 0.18
52..............................	1871	IC 3653	30.95 ± 0.06	...	30.84 ± 0.45	...
53..............................	9	IC 3019	31.17 ± 0.09	...	...	31.00 ± 0.10
57..............................	856	IC 3328	31.13 ± 0.07	...	...	31.28 ± 0.25
59..............................	1355	IC 3442	31.14 ± 0.08	...	...	30.92 ± 0.17
60..............................	1087	IC 3381	31.11 ± 0.06	...	...	31.27 ± 0.14
				...	...	31.39 ± 0.18
61..............................	1297	NGC 4486B	31.06 ± 0.07	31.14 ± 0.16	...	...

[a] Neilsen & Tsvetanov (2000).
[b] Tonry et al. (2001).
[c] Jerjen et al. (2004).

Figure 9 and Table 3 that the W′ cloud members bias the measured depth, leading to highly extended distributions along the line of sight. Excluding these galaxies gives a 1 σ dispersion in distance of ≈0.6 ± 0.1 Mpc, with no obvious dependence on luminosity class or color. Our best-estimate for the ±2 σ depth of the cluster is then 2.4 ± 0.4 Mpc, a range that should include 95% of Virgo's early-type galaxies. This range is about half the ±2 σ depth of 6 Mpc reported by Jerjen et al. (2004).

In the bottom panels of Figure 9, we show distance histograms for galaxies located within the nominal boundaries of the A and B subclusters (Binggeli et al. 1987). These two subclusters have distances that are identical, $d \approx 16.5$ Mpc, to within their measurement errors.

4.2. Distance-Velocity Distribution

The distance-velocity structure of the cluster is illustrated in Figure 10, which shows the ACSVCS galaxies, in the form of a gray-scale image (*left panel*) and as a surface plot (*right panel*). Two obvious substructures are apparent in this figure: (1) a large group between 15–18 Mpc and spread over a range of $\Delta v_r \sim$ 2000 km s^{-1} in radial velocity; and (2) a small group of five galaxies at ∼23 Mpc and ∼1100 km s^{-1} which belong to the W′ cloud. A third group of galaxies associated with M86 (VCC 881) may also be present at a mean distance of 17.6 ± 0.6 Mpc with a relative velocity of about −1000 km s^{-1} with respect to the cluster mean. However, in this case, the separation from the main component of the cluster is less extreme, and we cannot be certain without additional observations for an expanded sample of galaxies. We note that both Jerjen et al. (2004) and Schindler et al. (1999) have argued that M86 represents the dominant member of its own subcluster, albeit one much less massive than that associated with M87 (see Table 6 of Schindler et al. 1999).

Figure 11 shows a Hubble diagram for the ACSVCS sample, after transforming the heliocentric velocities into the CMB frame. Giants and dwarfs are shown separately as red circles and blue triangles. The five members of the W′ group are labeled explicitly, as are three galaxies (VCC 881, VCC 200, and VCC 1327) which may belong to the third association mentioned above. The straight dotted line drawn through the main concentration of galaxies shows an unperturbed Hubble flow for $H_0 = 73$ km s^{-1} Mpc^{-1}. The wavy solid curve passing through the cluster is the large-scale flow model of Tonry et al. (2000) for a line of sight passing
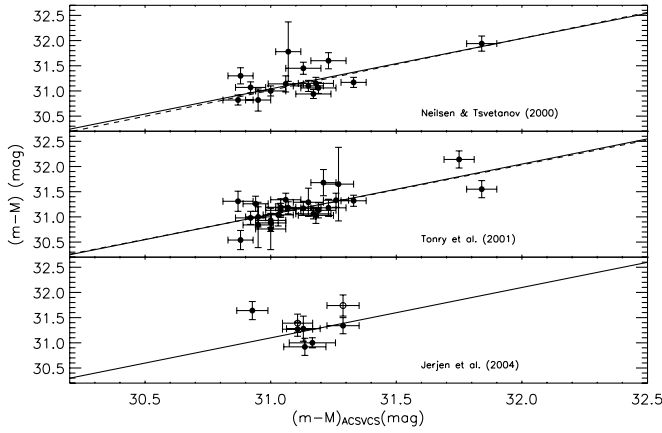
Fig. 6.—*Top*: Comparison of distance moduli from Neilsen & Tsvetanov (2000) with those from the ACSVCS for 15 Virgo galaxies in common between the two surveys. The solid line is the one-to-one relation, while the dashed line shows the line of best fit. *Middle panel;* Comparison of SBF distance moduli from Tonry et al. (2001) with those from the ACSVCS for 26 Virgo galaxies in common between the two surveys. The solid line is the one-to-one relation, while the dashed line shows the line of best fit. *Bottom:* Comparison of SBF distance moduli from Jerjen et al. (2004) with those from the ACSVCS for eight Virgo galaxies in common between the two surveys. For two galaxies (VCC 1087 = IC 3381 and VCC 1261 = NGC 4482), Jerjen et al. (2004) list two values for the distance modulus. In those cases, the higher measurements are shown by open circles. The dashed line has been calculated using the values from Jerjen et al. (2004) that agree best with our measurements (see Table 2). Note that the abscissa is stretched relative to the ordinate, and that the ACSVCS uncertainties are between one half and one tenth those of the ground-based measurements.
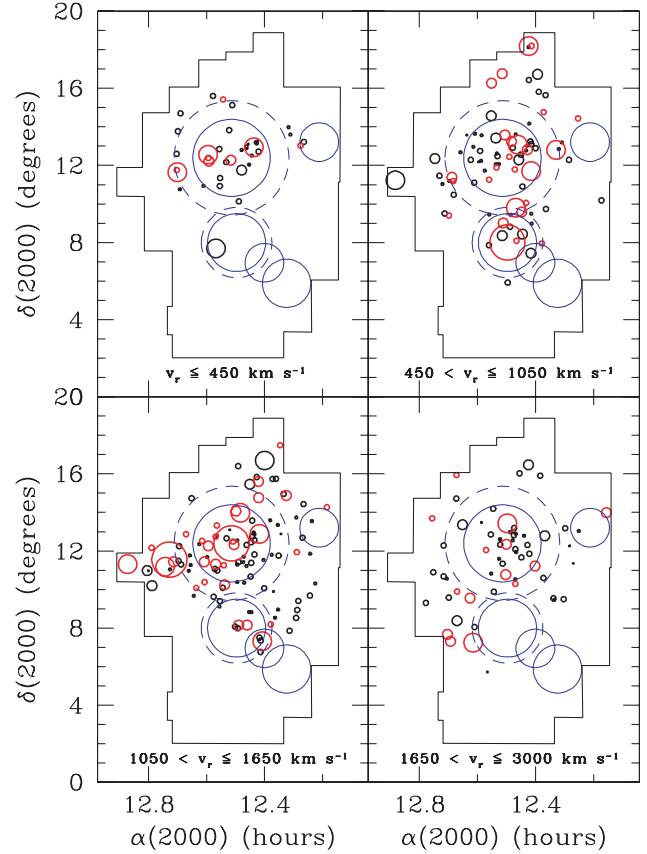

Fig. 8.—Distribution on the sky of 84 galaxies from the ACSVCS (*red circles*) with measured SBF distances, displayed in four ranges in heliocentric radial velocity: $v_r \leq 450\,\mathrm{km\,s^{-1}}$ (*top left*); $450 < v_r \leq 1050\,\mathrm{km\,s^{-1}}$ (*top right*); $1050 < v_r \leq 1650\,\mathrm{km\,s^{-1}}$ (*bottom left*); and $1650 < v_r \leq 3000\,\mathrm{km\,s^{-1}}$ (*bottom right*). Black circles show member galaxies with early-type morphologies from the VCC.

through the Virgo Cluster. This model includes the contribution of the Virgo Cluster (as well as the Great Attractor and a residual quadrupole) to the unperturbed Hubble flow.

The data and model are in good accord, particularly for the W' cloud, which has the expected infall velocity for its position. Moreover, the rms scatter about the mean relation is well described by the $\pm 1\,\sigma$ limits in the flow model (*dashed curves*). Figure 12 shows an expanded view of the region around the Virgo Cluster (i.e., over the range 4–40 Mpc), in which the ACSVCS data have been augmented by galaxies from the Tonry et al. (2001) survey, which lie within $20°$ of M87 and which were *not* included in the ACSVCS.[13] There is good agreement with the flow model on this larger scale as well.

Before proceeding, we comment on a curious feature of Figure 12. The distribution in the distance-velocity plane seems to be slightly inclined, in the sense that galaxies at high velocity tend to have larger distances while galaxies at low velocity tend to be on the near side of the cluster (excepting M86 and its likely companions). Such a correlation would be expected if the cluster has not yet virialized. Figure 13 shows a magnified view of the ACSVCS galaxies (with the W' cloud galaxies removed). A regression analysis of the remaining 79 galaxies shows that the inclination is not statistically significant. However a marginally significant correlation ($\sim 2\,\sigma$) is found if the three galaxies that
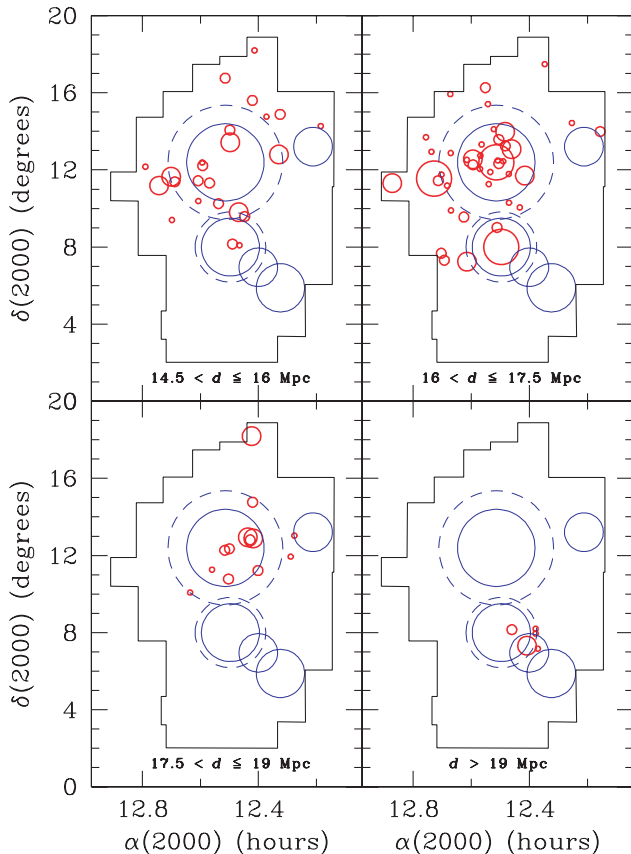

Fig. 7.—Distribution on the sky of 84 galaxies from the ACSVCS (*red circles*) with measured SBF distances, displayed in four ranges in distance: $14.5 < d \leq 16$ Mpc (*top left*); $16 < d \leq 17.5$ Mpc (*top right*); $17.5 < d \leq 19$ Mpc (*bottom left*); and $d > 19$ Mpc (*bottom right*).

[13] See Fig. 21 of Tonry et al. (2000) for an illustration of how the predicted Hubble flow relation depends on direction.
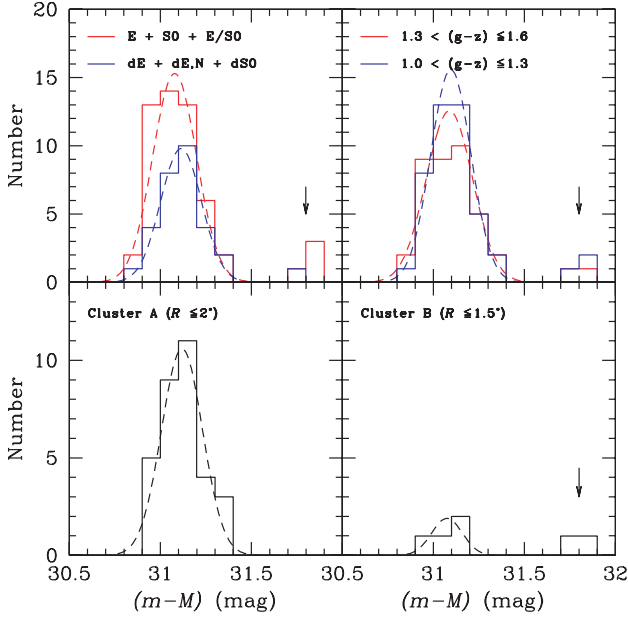
Fig. 9.—*Top:* Distribution of our measured SBF distances for 84 galaxies from the ACSVCS. The left panel shows the breakdown of the distance distributions by morphological type, while the right panel shows the breakdown by photometric color. The dashed curves show the best-fit Gaussian distributions. *Bottom:* Distribution of SBF distances for galaxies nominally within the boundaries of "cluster A" (projected separation <2′ from M87; *left*) and "cluster B" (projection separation <1.′5 from M49; *right panel*) defined by Binggeli et al. (1987, 1993). Note the presence of two galaxies (VCC 1025 = NGC 4434 and VCC 731 = NGC 4365), that fall inside the boundaries of cluster B but are actually associated with the W′ cloud at $d \sim 23$ Mpc (*arrows*).

may belong to the M86 (VCC 881) subcluster are omitted. The resulting best-fit linear relation and its $2\,\sigma$ confidence bands are shown as the long-dashed and dotted curves in Figure 13. If we also omit the two highest velocity galaxies, and thus fit the 74 main cluster galaxies in the velocity range $500 < v_{\rm CMB} < 2500$ km s^{-1}, then the significance reaches $2.6\,\sigma$, or 99%. This tentative correlation may be an echo of the cluster velocity distribution not yet having completely virialized. In the future, it will be interesting to test this possibility using SBF measurements for an expanded sample of galaxies.

4.3. *The Principal Axis of the Virgo Cluster*

Using SBF distances for 14 bright ellipticals from the catalog of Tonry et al. (2000, 2001), West & Blakeslee (2000) found that

the Virgo Cluster has a "principal axis" that extends roughly along the line of sight toward Abell 1367, part of the Coma supercluster, at $\alpha \approx 11^{\rm h}44.5^{\rm m}$, $\delta \approx 19.8°$ (J2000.0), $cz \approx 6600$ km s^{-1}, and $d \approx 90$ Mpc (e.g., Struble & Rood 1999; Sakai et al. 2000; Tully & Pierce 2000). The existence of a preferred axis for Virgo's bright elliptical galaxies had previously been noted by Arp (1968) and Binggeli et al. (1987). In this section we follow the analysis of West & Blakeslee (2000) using an expanded sample of more precise SBF distances, with the aim of determining the three-dimensional distribution of early-type Virgo galaxies, as traced by the ACSVCS sample. We remind the reader at the outset that the ACSVCS sample was chosen to give an unbiased view of the central $\sim 5°$ of the Virgo Cluster, but it excludes galaxies associated with some of the more interesting large-scale structures in the vicinity of Virgo (e.g., the Southern Extension, Ursa Major group, etc.). The shape and orientation that we will find in our analysis depend on the area coverage of our sample, and will be due to the all the substructures included in it.

As a starting point, right ascensions, declinations, and distances were used to define the Cartesian coordinates, in Mpc, for each of the 84 galaxies with SBF distances. The intrinsic standard deviations of the galaxy distribution (as defined in § 4.1) about these respective axes is then found to be $\sigma_i(\alpha) = 0.55 \pm 0.05$, $\sigma_i(\delta) = 0.67 \pm 0.07$, and $\sigma_i(d) = 1.62 \pm 0.41$ Mpc. Discarding the five galaxies at $d \approx 23$ Mpc, which are almost certainly members of the W′ cloud, one finds $\sigma_i(\alpha) = 0.55 \pm 0.05$ Mpc, $\sigma_i(\delta) = 0.62 \pm 0.06$, and $\sigma_i(d) = 0.62 \pm 0.06$ Mpc.

Figure 14 plots distance modulus against right ascension and declination for the ACSVCS galaxies (*red circles and blue triangles*). The open pentagons show the SBF measurements from Tonry et al. (2001), which were used by West & Blakeslee (2000) to show that the distance moduli of the brightest ellipticals vary with right ascension. This trend is not as obvious with our new sample, although a least-squares fit (*shown as the straight line in the top panel*) to our new measurements for the same sample of (bright) galaxies reveals a correlation consistent with the West & Blakeslee (2000) data. The dotted curves show the $2\,\sigma$ confidence bands on the fitted relation. It is not surprising that the correlation between distance modulus and right ascension is more diluted in our sample, since it includes galaxies over a much larger area than in West & Blakeslee (2000).

To better quantify the shape of the early-type galaxies in Virgo, we have calculated the inertia tensor of the galaxy distribution with respect to the cluster's center of mass. We have adopted as the fixed centroid of our galaxy distribution the point corresponding to average right ascension, declination, and distance

TABLE 3
MEAN DISTANCES AND DISPERSIONS FOR VIRGO CLUSTER SUBSAMPLES

| Sample	N	$\overline{(m-M)}$ (mag)	$\sigma(m-M)_o$ (mag)	$\overline{\sigma(m-M)}_m$ (mag)	$\sigma(m-M)_i$ (mag)	$\bar{d}$ (Mpc)	$\sigma(d)$ (Mpc)	$\bar{v}_r$ (km s^{-1})	σ_{v_r} (km s^{-1})
Giants	54	31.134 ± 0.031	0.227 ± 0.040	0.065	0.212	16.9 ± 0.2	1.7 ± 0.3	1107 ± 72	528 ± 53
Dwarfs	30	31.134 ± 0.029	0.156 ± 0.045	0.077	0.126	16.9 ± 0.2	1.0 ± 0.3	1180 ± 98	538 ± 64
$1.3 < (g_{475} - z_{850})_0 \leq 1.6$	39	31.124 ± 0.032	0.201 ± 0.045	0.066	0.183	16.8 ± 0.2	1.4 ± 0.3	1034 ± 87	541 ± 69
$1.0 \leq (g_{475} - z_{850})_0 \leq 1.3$	45	31.143 ± 0.031	0.208 ± 0.044	0.073	0.188	16.9 ± 0.2	1.5 ± 0.3	1218 ± 76	512 ± 45
Giants (no W′ cloud)	50	31.079 ± 0.017	0.120 ± 0.011	0.064	0.088	16.4 ± 0.1	0.7 ± 0.1	1116 ± 77	546 ± 55
Dwarfs (no W′ cloud)	29	31.114 ± 0.021	0.112 ± 0.013	0.076	0.065	16.7 ± 0.2	0.5 ± 0.1	1176 ± 102	547 ± 64
$1.3 < (g_{475} - z_{850})_0 \leq 1.6$ (no W′ cloud)	37	31.088 ± 0.021	0.127 ± 0.011	0.064	0.098	16.5 ± 0.2	0.7 ± 0.1	1027 ± 91	555 ± 70
$1.0 \leq (g_{475} - z_{850})_0 \leq 1.3$ (no W′ cloud)	42	31.096 ± 0.017	0.110 ± 0.012	0.066	0.072	16.6 ± 0.1	0.6 ± 0.1	1235 ± 80	521 ± 47
Cluster A ($R \leq 2°$)	32	31.119 ± 0.020	0.113 ± 0.012	0.071	0.072	16.7 ± 0.2	0.6 ± 0.1	1088 ± 105	593 ± 68
Cluster B ($R \leq 1.5°$)	4	31.075 ± 0.042	0.084 ± 0.020	0.066	0.014	16.4 ± 0.3	0.1 ± 0.1	958 ± 111	222 ± 94
W′ cloud	5	31.800 ± 0.029	0.065 ± 0.017	0.074	≤ 0.065	22.9 ± 0.3	≤ 0.7	1042 ± 113	253 ± 141
All Galaxies (no W′ cloud)	79	31.092 ± 0.013	0.118 ± 0.008	0.069	0.082	16.5 ± 0.1	0.6 ± 0.1	1138 ± 61	544 ± 40
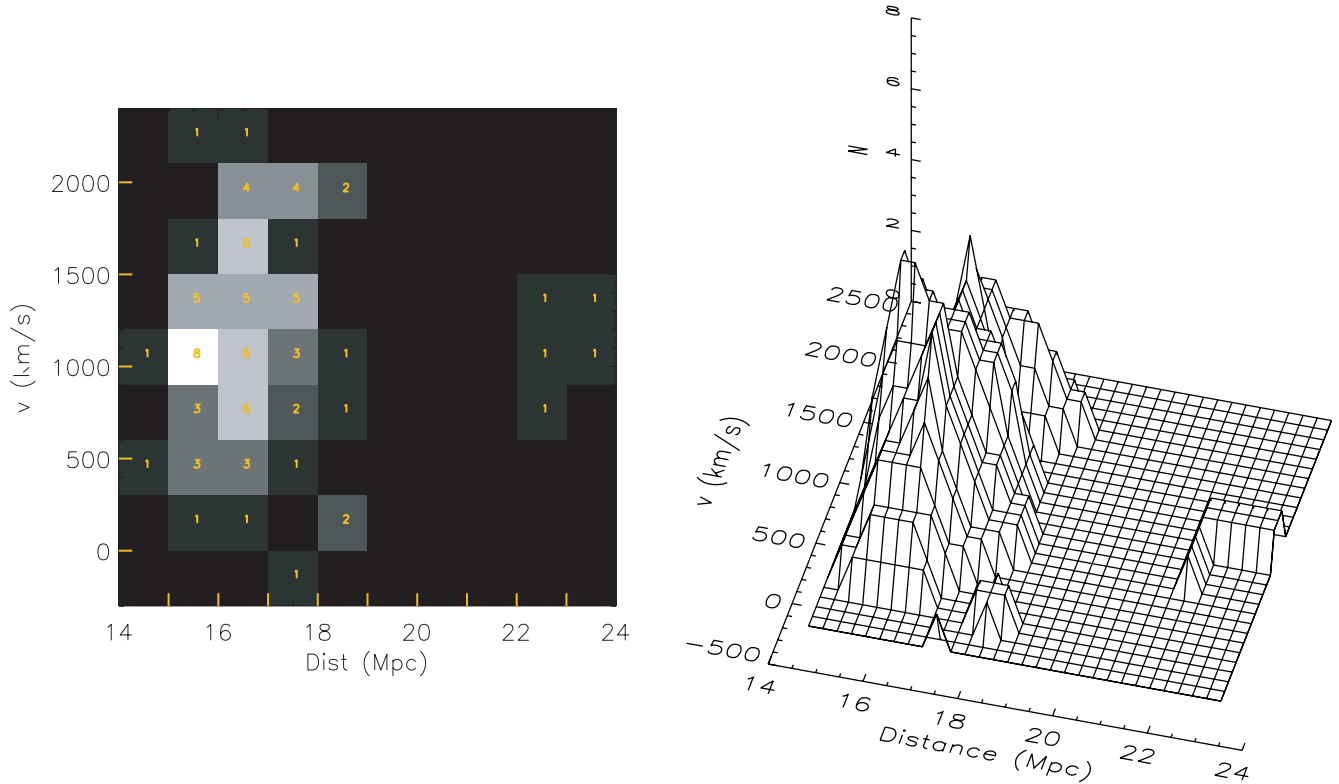
Fig. 10.— *Left:* Image showing a Hubble diagram for the ACSVCS sample, for 84 galaxies with measured SBF distances. The number of galaxies in each "pixel" has been labeled. *Right:* Surface plot for the preceding image.

(calculated by excluding the galaxies with $(m - M) > 31.5$ mag). The contributions to the scatter from observational error and cosmic variance can then be easily subtracted from the diagonal terms of the tensor to derive the intrinsic spatial distribution. The uncertainties in the distances are uncorrelated with the three positional variables.
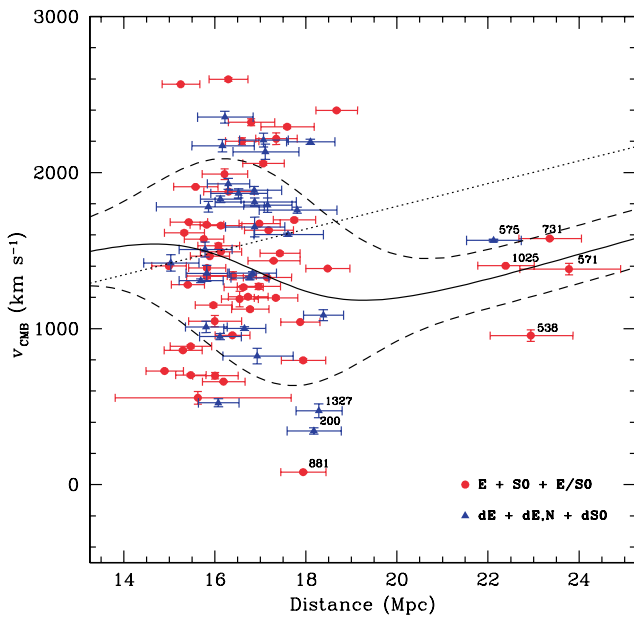
Fig. 11.— Velocity-distance relation for galaxies from the ACSVCS. Results for giants and dwarfs in the ACSVCS are shown separately as the red circles and blue triangles, respectively. The dotted lines shows the undisturbed Hubble Flow in the direction of Virgo for an assumed Hubble Constant of $H_0 = 73$ km s^{-1} Mpc^{-1}. The predicted distance-velocity relation for a line of sight passing through the cluster, based on the model of Tonry et al. (2000) for large-scale flows in the local universe, is shown by the solid (mean velocity) and dashed curves ($\pm 1 \sigma$ limits). Note the presence of five galaxies associated with the W' cloud at $D \approx 23$ Mpc. A third grouping of galaxies associated with VCC 881 (M86 = NGC 4406) may also be present, infalling from behind with a large negative radial velocity relative to the cluster mean.

Fig. 12.— Expanded view of the Hubble diagram shown in the previous figure. Over the distance range 4–40 Mpc, we plot giant and dwarf galaxies with measured SBF distances from the ACSVCS (*red circles and blue triangles*). Early-type galaxies from the SBF survey of Tonry et al. (2001), which are located with 20° of M87, and which do not appear in the ACSVCS, are plotted as open squares.

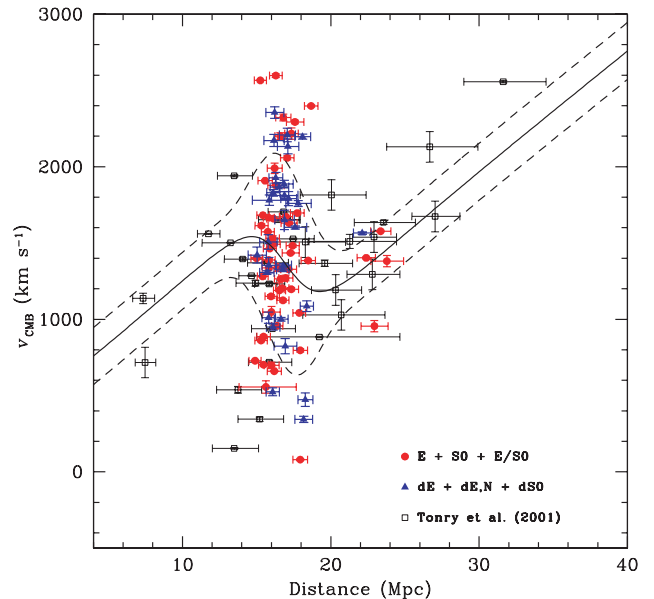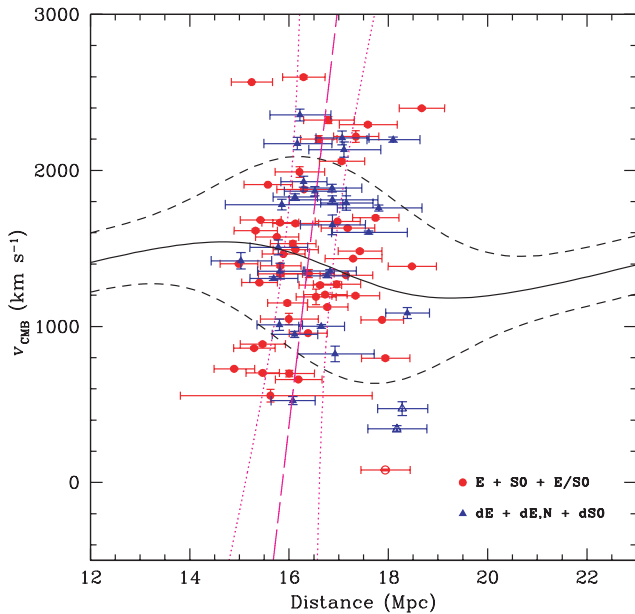FIG. 13.—Hubble diagram for the ACSVCS. The long-dashed line shows a linear least-squares fit to the measured velocities and distances, excluding five members of the W' cloud (not shown) and the three galaxies (*open symbols*) that may belong to the VCC 881 subcluster (i.e., 76 galaxies in total). The 2 σ confidence bands on the fitted relation are shown by the dotted curves.

The principal axes of the galaxy distribution are then given by the eigenvectors of the inertia tensor; these axes identify the major, minor and intermediate axes of the ellipsoid that best fits the galaxy distribution. The elongation along these axes are given by the eigenvalues of the tensor.

In Table 4 shape parameters for the galaxy distribution are shown as the major-, intermediate-, and minor-axis ratios—a, b, and c, respectively—after normalizing to the major axis. These values and their uncertainties were obtained by bootstrapping on 1000 simulations of each of our samples. As an illustration, with this parameterization, a straight line would have $(a, b, c) = (1, 0, 0)$ and a sphere would have $(1, 1, 1)$. Excluding the five probable members of the W' cloud, which have $(m - M) > 31.5$ mag, gives axis ratios of $(1.0, 0.7, 0.5)$. These values are representative of those found for various subsets of the 79 galaxies with $(m - M) < 31.5$ mag, after dividing the sample on the basis of color, luminosity, and/or morphological type (i.e., giants vs. dwarfs). If one chooses to weight the sample by luminosity, the ratios typically change by ~30% percent, approaching the distribution of the brightest ($M_B < 12$ mag) galaxies, which has a more elongated distribution with respect to the total distribution.

Figure 15 shows the sample distribution in supergalactic coordinates, with red circles indicating the brightest galaxies in the sample ($M_B < 12$ mag). Supergalactic coordinates have their equator aligned with the supergalactic plane, defined by de Vaucouleurs (1961) as the plane in which most of the structures belonging to the local supercluster (centered on the Virgo Cluster) lie. In particular, the origin of the spherical supergalactic coordinate system (SGB $= 0°$, SGL $= 0°$) lies at galactic coordinates $l = 137.37°$, $b = 0°$; that is $\alpha \sim 42°$ and $\delta \sim +59.5°$ (J2000.0), with the north pole at galactic coordinates $l = 47.37°$, $b = +6.32°$. We projected the spherical supergalactic coordinates to a Cartesian plane. The galaxy distribution is significantly flattened in the SGZ direction.

In summary, the distribution of our sample of early-type Virgo galaxies appears triaxial, although with only a mild elongation along the major axis. This conclusion is largely independent of
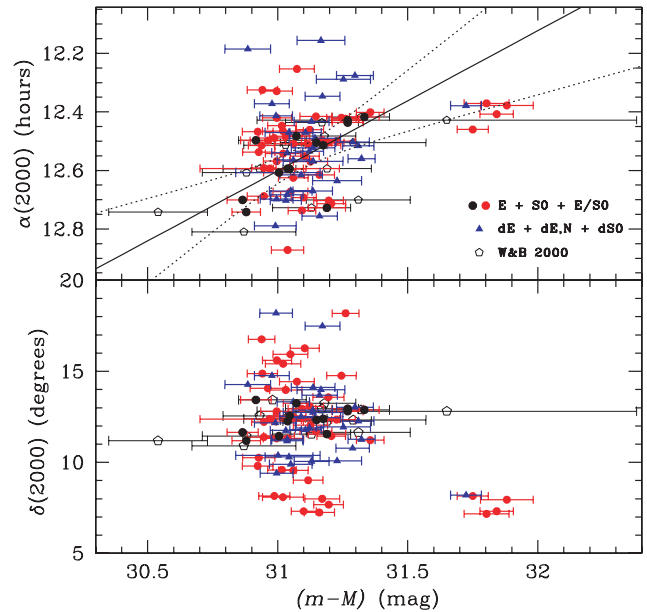

FIG. 14.—*Top*: Distance modulus plotted against right ascension for galaxies from the ACSVCS. Dwarf and giant galaxies are shown by the blue triangles and red circles, respectively. Open pentagons show the sample of galaxies (with SBF measurements from Tonry et al. 2001) used by West & Blakeslee (2000) to define Virgo's principal axis; our measurements for these galaxies are shown as the black circles. The straight line and dotted curves show the best-fit linear relation and 2 σ confidence bands based on our SBF distances for these galaxies. *Bottom*: Distance modulus plotted against declination for galaxies from the ACSVCS. The symbols are the same as in the above panel.

galaxy color and morphological classification, with the dwarfs and giants having similar triaxial distributions. As shown in Table 4, the principal axis of the early-type galaxy distribution is found to be inclined at an angle of ~20°–70° to the line of sight to the cluster (i.e., elongated roughly along the direction to the cluster), with the precise inclination depending on the sample definition. In particular, if the sample is not restricted to exclude the five members of the background W' cloud, then a much more elongated distribution is found: i.e., $(1, 0.4, 0.3)$, inclined at an angle of ~10°. The background W cloud, at roughly twice the distance of Virgo, appears to connect to the cluster via a filament (that includes the W' cloud) wrapping around a background "void" and connecting with the Virgo Southern Extension (R. Tully 2006, private communication). A larger elongation is also observed for the brightest galaxies ($M_B < 12$ mag), at an angle of ~30° $\pm$ 20° to the line of sight.

5. CONCLUSIONS

SBF distances from the ACS Virgo Cluster Survey offer the best opportunity to date to map out the three-dimensional distribution of early-type galaxies within the Virgo Cluster. The final sample of 84 galaxies (50 giants and 34 dwarfs) with SBF distances from this survey nearly triples the number of Virgo Cluster galaxies with available SBF distances. At the same time, the new z_{850}-band SBF magnitudes and distances have a typical (internal) precision of ≈ 0.07 mag and ≈ 0.5 Mpc—roughly a factor of 3 improvement over previous measurements. An illustration of the three-dimensional distribution of our program galaxies within the Virgo Cluster is presented in Figure 16.

Five galaxies in the survey (VCC 538, VCC 571, VCC 575, VCC 731, and VCC 1025) lie well behind the Virgo Cluster, at a mean distance of $d \approx 22.9 \pm 0.3$ Mpc. These galaxies are almost

TABLE 4
AXES OF THE THREE-DIMENSIONAL GALAXY DISTRIBUTION

Sample	N	a	b	c	Θ (deg)
Unweighted					
All galaxies	84	1	0.43 ± 0.09	0.27 ± 0.06	12 ± 2
Galaxies with $(m-M) < 31.5$	79	1	0.74 ± 0.08	0.48 ± 0.05	29 ± 29
Giants with $(m-M) < 31.5$	50	1	0.68 ± 0.09	0.41 ± 0.06	21 ± 21
Dwarfs with $(m-M) < 31.5$	29	1	0.74 ± 0.12	0.42 ± 0.11	65 ± 30
Galaxies with $(g_{475} - z_{850})_0 \leq 1.3$ and $(m-M) < 31.5$	42	1	0.79 ± 0.09	0.50 ± 0.09	54 ± 41
Galaxies with $(g_{475} - z_{850})_0 > 1.3$ and $(m-M) < 31.5$	37	1	0.62 ± 0.10	0.38 ± 0.06	24 ± 17
Galaxies with $M_B < 12$ mag and $(m-M) < 31.5$	17	1	0.55 ± 0.11	0.35 ± 0.09	30 ± 16
Galaxies with $M_B < 12$ mag, $(m-M) < 31.5$ and $\delta(2000) > 10^o$	14	1	0.48 ± 0.12	0.25 ± 0.12	28 ± 15
Galaxies WB	15	1	0.28 ± 0.04	0.12 ± 0.05	12 ± 3
Galaxies with $M_B > 15$ mag and $(m-M) < 31.5$	15	1	0.73 ± 0.13	0.22 ± 0.11	69 ± 38
Galaxies with $\delta(2000) > 10^o$	67	1	0.69 ± 0.08	0.40 ± 0.06	26 ± 25
Luminosity Weighted					
All galaxies	84	1	0.46 ± 0.16	0.26 ± 0.10	16 ± 15
Galaxies with $(m-M) < 31.5$	79	1	0.68 ± 0.12	0.41 ± 0.10	42 ± 33
Giants with $(m-M) < 31.5$	50	1	0.65 ± 0.13	0.38 ± 0.09	33 ± 29
Dwarfs with $(m-M) < 31.5$	29	1	0.70 ± 0.13	0.39 ± 0.11	63 ± 31
Galaxies with $(g_{475} - z_{850})_0 \leq 1.3$ and $(m-M) < 31.5$	42	1	0.74 ± 0.11	0.46 ± 0.10	56 ± 36
Galaxies with $(g_{475} - z_{850})_0 > 1.3$ and $(m-M) < 31.5$	37	1	0.62 ± 0.13	0.35 ± 0.09	28 ± 23
Galaxies with $M_B < 12$ mag and $(m-M) < 31.5$	17	1	0.57 ± 0.14	0.33 ± 0.11	34 ± 23
Galaxies with $M_B < 12$ mag, $(m-M) < 31.5$ and $\delta(2000) > 10^o$	14	1	0.50 ± 0.15	0.25 ± 0.12	31 ± 18
Galaxies WB	15	1	0.32 ± 0.08	0.10 ± 0.06	15 ± 5
Galaxies with $M_B > 15$ mag and $(m-M) < 31.5$	15	1	0.64 ± 0.15	0.25 ± 0.09	61 ± 31
Galaxies with $\delta(2000) > 10^\circ$	67	1	0.64 ± 0.13	0.36 ± 0.09	38 ± 30

NOTES.—The parameters a, b, and c are, respectively, the main, intermediate and minor axis of the distribution, normalized to the length of the main axis. N is the number of galaxies in each sample. The orientation angle, Θ, is the angle between the line of sight and the main axis. "WB" refers to a sample selected to be more similar to the West & Blakeslee sample, with $B_T < 12.93$ mag, right ascension between 12.65^h and 12.35^h and declination between 10.5° and 14.5°.

certainly members of the W′ cloud. Binggeli et al. (1993) have previously described this structure as a filament, viewed nearly end-on, that connects the Virgo B subcluster with the background W cloud (at roughly twice the distance of the Virgo Cluster). Our finding that these five galaxies occupy such an apparently narrow
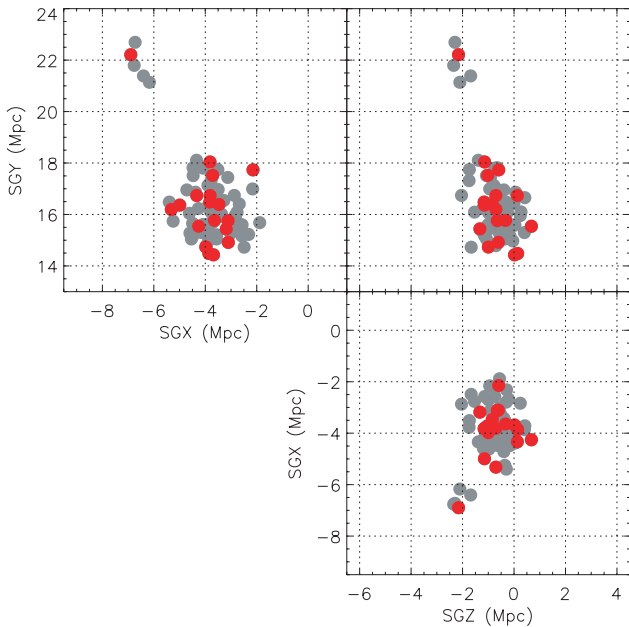
FIG. 15.—ACSVCS galaxy spatial distribution plotted in supergalactic Cartesian coordinates, with the SGY axis being approximately along the line of sight. The left panel shows the view from "above" the supergalactic plane, with the SGY axis being along the line of sight. The right panels give the view within the plane. The brightest ellipticals ($B_T < 12$ mag), are plotted in red.

FIG. 16.—Three-dimensional distribution of our program galaxies within the Virgo Cluster. The cluster is embedded in a rectangular parallelepiped of dimensions $4 \times 4 \times 9.5$ Mpc. The red spheres show galaxies with $B_T \leq 12$ mag. The direction of the Milky Way is indicated by the arrow.

range in distance (to within the errors, there is no evidence for any spread in distance at all) suggests that the W′ cloud may be a more localized structure than previously believed.

Excluding these background W′ galaxies, we find the remaining sample of 79 galaxies to occupy a narrow range in distance, with a mean of $d = 16.5 \pm 0.1$ (ran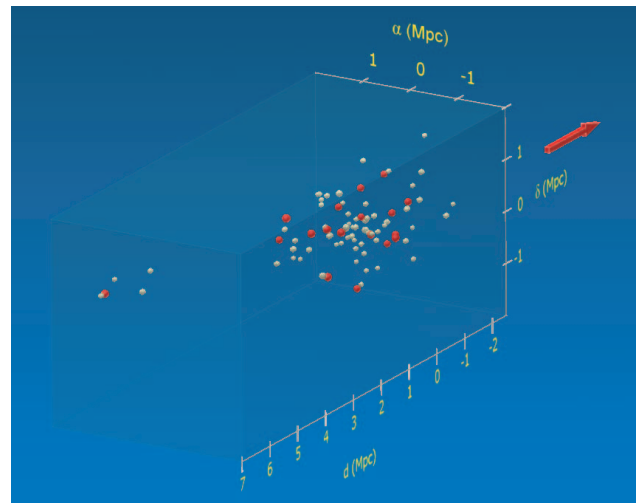dom) ± 1.1 Mpc (systematic). After accounting for measurement errors and cosmic scatter, we find the $1\,\sigma$ dispersion in distance to be $\sigma(d) = 0.6 \pm 0.1$ Mpc. Our estimate for the back-to-front depth of the cluster is then $\approx 2.4 \pm 0.4$ Mpc (i.e., $\pm 2\,\sigma$ of the distance distribution: a range that should encompass 95% of the cluster's early-type galaxies). This finding is clearly at odds with some claims of much more elongated distributions found using less precise distance indicators (e.g., Young & Currie 1995). At the same time, however, our carefully chosen sample turned out to include five members of the W′ cloud, despite the fact that all were considered certain Virgo members in the VCC (Binggeli et al. 1985). Although ground-based SBF measurements (Tonry et al. 1990, 2001) had already placed NGC 4365 (VCC 731) and NGC 4434 (VCC 1025) in the background toward the direction of the W cloud, the existence of such a compact, distinct physical grouping displaced by ∼6 Mpc from the main body of the cluster would almost certainly have gone unrecognized in studies using distances of precision ∼3 Mpc. We therefore suspect that contamination by galaxies lying in the immediate cluster background may at least partly account for the elongated distributions reported by some previous researchers. We also note that, due to our sample definition, these background galaxies would not have been included in the sample if the distance offset were perpendicular to the line of sight (as is the case for the Virgo Southern Extension), rather than along it.

Parsing the sample of early-type galaxies by morphological type, luminosity, and color reveals no large differences in distribution, although there is some evidence that the giants may have a slightly more elongated distribution than the dwarfs (0.7 ± 0.1 Mpc vs. 0.5 ± 0.1 Mpc). We emphasize that these measurements are based on *early-type* galaxies, which are known to be more concentrated toward the cluster center than the late-type systems. Our SBF measurements show that the well-known A and B subclusters (defined by M87 and M49, respectively) lie at a nearly identical distance of $d \approx 16.5$ Mpc. A small number of the galaxies in our survey may belong to a third subcluster, about 1 Mpc more distant, associated with M86 (see also Schindler et al. 1999; Jerjen et al. 2004).

A tensor of inertia analysis is used to examine the three-dimensional distribution of early-type galaxies in the Virgo Cluster. We find the main body of the cluster to have a mildly triaxial shape, with axial ratios of (1, 0.7, and 0.5). If the five W′ cloud galaxies are included in the solution, then the axial ratios become (1, 0.4, 0.3), because these galaxies do not lie in the center of the cluster as most of the galaxies of the sample.

The principal axis of this distribution is inclined by ∼20°–40° from the line of sight.

While our conclusions are robust to the precise choice of SBF calibration (see the Appendix), in the future we plan to refine our adopted calibration using SBF measurements for a sample of ∼40 galaxies in the Fornax Cluster (e.g., Jordán et al. 2005b about our Fornax Cluster Survey (FCS); Dunn & Jerjen 2006 about the use of SBF in measuring distances in the Fornax cluster). Because it is much more compact than Virgo (Tonry et al. 1997), the SBF magnitudes measured in Fornax galaxies will allow a more direct and straightforward calibration of the $\overline{M}_{850} - (g_{475} - z_{850})_0$ relation. A forthcoming paper in this series will use our SBF distances to re-assess the accuracy of several distance indicators commonly used to derive distances for early-type galaxies.

APPENDIX

CHOICE OF CALIBRATION

To understand the uncertainties inherent to the choice of SBF calibration, we compare the results obtained using the broken-linear relation of equation (1) with two other possible calibrations: a single-slope linear fit and a fourth-order polynomial fit.

The calibration by equation (1) was chosen to minimize the χ^2 of a fit of SBF measurements as a function of $(g_{475} - z_{850})_0$ for 84 galaxies, in two color regimes divided at $(g_{475} - z_{850})_0 = 1.3$ mag. Using the same sample and the least-squares fitting technique, the best-fit linear calibration is

$$\overline{M}_{850} = -2.00 \pm 0.04 + (1.3 \pm 0.1)[(g_{475} - z_{850})_0 - 1.3], \quad \text{if } 1.0 \leq (g_{475} - z_{850})_0 \leq 1.6, \tag{A1}$$

while a fourth-order polynomial fit gives

$$\begin{aligned}\overline{M}_{850} = &-2.04 \pm 0.05 + (1.12 \pm 0.36)x + (1.97 \pm 2.00)x^2 \\ &+ (8.38 \pm 8.28)x^3 + (11.33 \pm 23.46)x^4, \quad \text{if } 1.0 \leq (g_{475} - z_{850})_0 \leq 1.6,\end{aligned} \tag{A2}$$

with $x = [(g_{475} - z_{850})_0 - 1.3]$. In equation (A2), we approximate the errors on the polynomial coefficients as the square root of the diagonal terms of the fit covariance matrix. Distance moduli derived from the three different calibrations are presented in Table 5, and

TABLE 5
DISTANCE MODULI FOR DIFFERENT SBF CALIBRATIONS

ID No.	VCC No.	$(m-M)_{\mathrm{bl}}$ (mag)	$(m-M)_l$ (mag)	$(m-M)_p$ (mag)
1......................................	1226	31.17 ± 0.07	31.26 ± 0.04	31.14 ± 0.05
2......................................	1316	31.17 ± 0.07	31.27 ± 0.04	31.12 ± 0.06
3......................................	1978	31.19 ± 0.07	31.31 ± 0.04	31.06 ± 0.06
4......................................	881	31.27 ± 0.06	31.32 ± 0.03	31.30 ± 0.05
5......................................	798	31.26 ± 0.05	31.23 ± 0.03	31.27 ± 0.05
6......................................	763	31.33 ± 0.06	31.36 ± 0.03	31.37 ± 0.05
7......................................	731	31.84 ± 0.06	31.91 ± 0.04	31.84 ± 0.05
9......................................	1903	30.86 ± 0.06	30.92 ± 0.03	30.89 ± 0.05
10......................................	1632	31.05 ± 0.06	31.12 ± 0.04	31.05 ± 0.05
11......................................	1231	30.92 ± 0.06	30.96 ± 0.04	30.95 ± 0.05
13......................................	1154	31.03 ± 0.06	31.08 ± 0.04	31.06 ± 0.05
14......................................	1062	30.92 ± 0.06	30.96 ± 0.04	30.96 ± 0.05
15......................................	2092	31.04 ± 0.06	31.09 ± 0.04	31.06 ± 0.05
16......................................	369	31.00 ± 0.06	31.03 ± 0.04	31.03 ± 0.05
17......................................	759	31.15 ± 0.06	31.20 ± 0.04	31.17 ± 0.05
18......................................	1692	31.16 ± 0.06	31.19 ± 0.04	31.19 ± 0.05
19......................................	1030	31.12 ± 0.05	31.07 ± 0.03	31.10 ± 0.05
20......................................	2000	30.88 ± 0.05	30.84 ± 0.04	30.88 ± 0.05
22......................................	1664	31.00 ± 0.06	31.03 ± 0.04	31.04 ± 0.05
24......................................	944	31.02 ± 0.05	31.01 ± 0.03	31.04 ± 0.05
25......................................	1938	31.21 ± 0.05	31.15 ± 0.04	31.18 ± 0.05
26......................................	1279	31.15 ± 0.06	31.16 ± 0.04	31.18 ± 0.05
27......................................	1720	31.06 ± 0.06	31.08 ± 0.04	31.09 ± 0.05
28......................................	355	30.94 ± 0.06	30.95 ± 0.04	30.97 ± 0.05
29......................................	1619	30.95 ± 0.05	30.89 ± 0.03	30.92 ± 0.05
30......................................	1883	31.10 ± 0.05	31.05 ± 0.04	31.07 ± 0.05
31......................................	1242	30.96 ± 0.07	30.91 ± 0.05	30.94 ± 0.06
32......................................	784	31.00 ± 0.06	30.98 ± 0.04	31.01 ± 0.05
33......................................	1537	31.00 ± 0.05	30.94 ± 0.04	30.97 ± 0.05
34......................................	778	31.25 ± 0.06	31.20 ± 0.04	31.23 ± 0.05
35......................................	1321	30.94 ± 0.05	30.89 ± 0.04	30.91 ± 0.05
36......................................	828	31.27 ± 0.06	31.26 ± 0.04	31.29 ± 0.05
37......................................	1250	31.23 ± 0.07	31.23 ± 0.06	31.22 ± 0.07
38......................................	1630	31.04 ± 0.06	31.06 ± 0.04	31.07 ± 0.05
39......................................	1146	31.07 ± 0.05	31.02 ± 0.04	31.05 ± 0.05
40......................................	1025	31.75 ± 0.06	31.75 ± 0.04	31.77 ± 0.05
41......................................	1303	31.12 ± 0.06	31.09 ± 0.04	31.13 ± 0.05
42......................................	1913	31.20 ± 0.06	31.16 ± 0.04	31.19 ± 0.05
43......................................	1327	31.27 ± 0.07	31.28 ± 0.05	31.30 ± 0.06
45......................................	1475	31.10 ± 0.06	31.08 ± 0.04	31.09 ± 0.05
46......................................	1178	30.99 ± 0.06	30.98 ± 0.04	31.01 ± 0.05
47......................................	1283	31.19 ± 0.06	31.19 ± 0.04	31.22 ± 0.05
48......................................	1261	31.29 ± 0.06	31.30 ± 0.05	31.29 ± 0.06
49......................................	698	31.36 ± 0.05	31.30 ± 0.04	31.33 ± 0.05
50......................................	1422	30.93 ± 0.06	30.91 ± 0.05	30.92 ± 0.06
52......................................	1871	30.95 ± 0.06	30.93 ± 0.05	30.96 ± 0.06
53......................................	9	31.17 ± 0.09	31.20 ± 0.08	31.18 ± 0.08
54......................................	575	31.72 ± 0.06	31.68 ± 0.05	31.70 ± 0.06
55......................................	1910	31.03 ± 0.06	30.99 ± 0.04	31.02 ± 0.05
56......................................	1049	31.02 ± 0.08	31.06 ± 0.06	31.03 ± 0.07
57......................................	856	31.13 ± 0.07	31.12 ± 0.05	31.12 ± 0.06
58......................................	140	31.07 ± 0.07	31.08 ± 0.05	31.07 ± 0.06
59......................................	1355	31.14 ± 0.08	31.15 ± 0.07	31.14 ± 0.08
60......................................	1087	31.11 ± 0.06	31.07 ± 0.05	31.09 ± 0.06
61......................................	1297	31.06 ± 0.07	31.11 ± 0.05	31.09 ± 0.06
62......................................	1861	31.04 ± 0.06	30.99 ± 0.05	31.01 ± 0.06
63......................................	543	30.98 ± 0.07	30.97 ± 0.05	30.97 ± 0.06
64......................................	1431	31.04 ± 0.06	30.98 ± 0.05	31.01 ± 0.06
65......................................	1528	31.06 ± 0.06	31.03 ± 0.05	31.04 ± 0.06
66......................................	1695	31.09 ± 0.08	31.13 ± 0.06	31.10 ± 0.07
67......................................	1833	31.05 ± 0.07	31.05 ± 0.05	31.05 ± 0.06
68......................................	437	31.17 ± 0.07	31.15 ± 0.06	31.16 ± 0.06
69......................................	2019	31.16 ± 0.07	31.16 ± 0.05	31.16 ± 0.06
70......................................	33	30.89 ± 0.09	30.94 ± 0.06	30.90 ± 0.08
71......................................	200	31.30 ± 0.07	31.29 ± 0.06	31.29 ± 0.07

TABLE 5—*Continued*

ID No.	VCC No.	$(m - M)_{bl}$ (mag)	$(m - M)_l$ (mag)	$(m - M)_p$ (mag)
72......................................	571	31.88 ± 0.10	31.92 ± 0.09	31.89 ± 0.09
76......................................	1895	31.00 ± 0.06	31.01 ± 0.04	31.00 ± 0.05
78......................................	1545	31.13 ± 0.07	31.08 ± 0.06	31.10 ± 0.07
81......................................	1075	31.04 ± 0.09	31.04 ± 0.08	31.04 ± 0.09
83......................................	1627	30.78 ± 0.06	30.81 ± 0.04	30.82 ± 0.05
84......................................	1440	31.02 ± 0.07	31.01 ± 0.06	31.01 ± 0.06
85......................................	230	31.25 ± 0.10	31.25 ± 0.10	31.25 ± 0.10
86......................................	2050	30.99 ± 0.08	31.01 ± 0.07	31.00 ± 0.07
88......................................	751	30.99 ± 0.06	30.95 ± 0.05	30.97 ± 0.06
87......................................	1993	31.09 ± 0.05	31.06 ± 0.04	31.07 ± 0.05
89......................................	1828	31.14 ± 0.08	31.12 ± 0.07	31.12 ± 0.07
90......................................	538	31.80 ± 0.09	31.82 ± 0.07	31.81 ± 0.08
91......................................	1407	31.12 ± 0.05	31.09 ± 0.04	31.10 ± 0.05
94......................................	1743	31.23 ± 0.09	31.26 ± 0.08	31.24 ± 0.09
95......................................	1539	31.14 ± 0.12	31.14 ± 0.11	31.13 ± 0.11
96......................................	1185	31.14 ± 0.10	31.11 ± 0.09	31.12 ± 0.10
97......................................	1826	31.05 ± 0.08	31.06 ± 0.07	31.05 ± 0.08
98......................................	1512	31.32 ± 0.05	31.27 ± 0.04	31.30 ± 0.05
100......................................	1661	31.00 ± 0.16	30.96 ± 0.16	30.98 ± 0.16

Notes.—Distance moduli: $(m - M)_{bl}$ = broken linear relation; $(m - M)_l$ = single linear relation; $(m - M)_p$ = polynomial relation.

galaxy-by-galaxy differences in distance modulus obtained using equations (A1) or equation (A2), rather than equation (1), are shown in the top panel of Figure 17. For reference, the bottome panel of this figure shows the adopted distance moduli plotted against galaxy color. There is no trend with either color or morphological type, supporting the validity of the broken linear calibration adopted in § 3.2.

In performing these fits, we add two additional sources of uncertainty to the errors on the SBF magnitudes. The first is an "uncertainty" of 0.11 mag, introduced to account for the actual distance dispersion caused by the line-of-sight depth of the cluster. This value was adopted based on the rms scatter of the angular distances measured within ∼3° in position on the sky of the 100 ACSVCS program galaxies. The second uncertainty is the expected "cosmic scatter" of 0.05 mag in fluctuation magnitude (see Tonry et al. 1997), representing the intrinsic dispersion in $\overline{M}_{850}$ for galaxies at a fixed color.

The three different calibrations are shown in the bottom panel of Figure 5, and their normalized χ^2 and scatters are given in Table 6 for the 79 galaxies having distance moduli of $(m - M) < 31.5$ mag. Note that the normalized χ^2 are larger than expected when we do not include the uncertainties due to depth effects in the Virgo Cluster and the intrinsic dispersion in $\overline{M}_{850}$. When these sources of scatter are
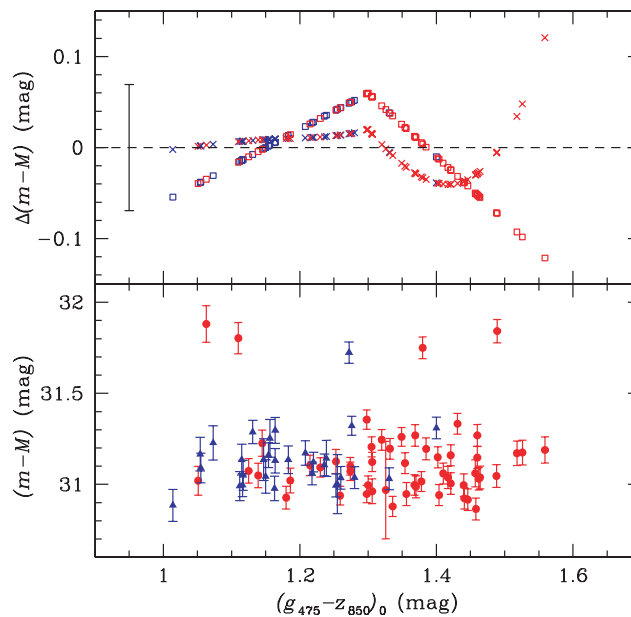

Fig. 17.— *Top:* Differences between distance moduli derived with the broken linear calibration (eq. [1]) and the single linear (eq. [A1]; *squares*) and polynomial calibrations (eq. [A2]; *crosses*). Red and blue symbols show galaxies classified as giants and dwarfs, respectively, by Binggeli et al. (1985). The error bar indicates the mean random error, $\sigma(m - M) = 0.069$ mag, on the measured distance moduli. *Bottom:* Distance moduli as a function of galaxy color. Red circles and blue triangles are used for giants and dwarfs, respectively. The distance moduli show no correlation with color, supporting the validity of the adopted SBF calibration.

TABLE 6
Comparison of SBF Calibrations

Relation	N	χ_r^{2}[a]	χ_d^{2}[a]	σ[b] (mag)	$\|(m-M)_{\rm bl} - (m-M)\|$[c] (mag)
Broken linear	79	28.5	0.91	0.12	...
Linear	79	36.7	0.99	0.12	0.03 ± 0.02
Polynomial	79	28.1	0.91	0.12	0.02 ± 0.02
Broken linear $(g_{475}-z_{850})_0 \le 1.5$................	76	27.3	0.93	0.12	...
Linear $(g_{475}-z_{850})_0 \le 1.5$...........................	76	27.1	0.93	0.12	0.03 ± 0.02
Polynomial $(g_{475}-z_{850})_0 \le 1.5$.....................	76	28.9	0.95	0.12	0.02 ± 0.01

[a] The values χ_r^2 and χ_d^2 are the reduced χ^2 of the fits and the reduced χ^2 when taking into account the uncertainties due to depth effects in the Virgo Cluster (0.11 mag) and the "cosmic" dispersion in $\overline{M}_{850}$ (0.05 mag).
[b] The rms scatter around the fitted relation.
[c] Average absolute difference relative to the broken linear (bl) relation.

taken into account, χ^2 has values around unity. Although the χ^2 for the polynomial fit is slightly lower when the full galaxy sample is considered, it increases for the subset of galaxies with $(g_{475}-z_{850})_0 < 1.5$ mag. This is because the polynomial calibration gives a better match to those few galaxies with $(g_{475}-z_{850})_0 > 1.5$ mag.

In fact, the three brightest and reddest galaxies in our sample—all with $(g_{475}-z_{850})_0 > 1.5$ mag—have SBF magnitudes slightly larger (but always within $1\,\sigma$) than expected if they lie at the precise center of the cluster. As a consequence, equation (1) yields distance moduli which are ≈ 0.08 mag larger than the mean Virgo distance for these three galaxies (M87, M49, and M60). While this modest offset may represent a real dislocation of these three galaxies from the cluster center, it may also be an artifact of the choice of SBF calibration, i.e., the steepening of the SBF–color relation for the very reddest galaxies may be real. The composite stellar population models presented by Blakeslee et al. (2001) showed such a steepening of the I-band SBF relation for very metal-rich populations (see also Fig. 7 of Paper V, showing Bruzual & Charlot 2003 SSP models for the F850LP bandpass). In any case, the average uncertainty in distance modulus is 0.07 mag, so that distance moduli derived using the different calibrations are always consistent with the $1\,\sigma$ errors, with the exception of VCC 1978 (M60)—the reddest galaxy in the sample. Nevertheless, we advise future users of the SBF distance catalog to exercise caution by comparing all three distance sets to test for robustness against the choice of calibration.

REFERENCES

Ajhar, E. A., Lauer, T. R., Tonry, J. L., Blakeslee, J. P., Dressler, A., Holtzman, J. A., & Postman, M. 1997, AJ, 114, 626
Ajhar, E. A., Tonry, J. L., Blakeslee, J. P., Riess, A. G., & Schmidt, B. P. 2001, ApJ, 559, 584
Arp, H. 1968, PASP, 80, 129
Binggeli, B. 1999, in The Radio Galaxy Messier 87, ed. H.-J. Röser & K. Meisenheimer (Berlin: Springer), 9
Binggeli, B., Popescu, C. C., & Tammann, G. A. 1993, A&AS, 98, 275
Binggeli, B., Sandage, A., & Tammann, G. A. 1985, AJ, 90, 1681
Binggeli, B., Tammann, G. A., & Sandage, A, 1987, AJ, 94, 251
Bird, C. M. 1994, AJ, 107, 1637
Blakeslee, J. P., Ajhar, E. A., & Tonry, J L. 1999, in Post-Hipparcos Cosmic Candles, ed. A. Heck & F. Caputo (Boston: Kluwer), 181
Blakeslee, J. P., Lucey, J. R., Tonry, J. L., Hudson, M. J., Narayanan, V. K., & Barris, B. J. 2002, MNRAS, 330, 443
Blakeslee, J. P., Vazdekis, A., & Ajhar, E. A. 2001, MNRAS, 320, 193
Böhringer, H., Briel, U. G., Schwarz, R. A., Voges, W., Hartner, G., & Trumper, J. 1994, Nature, 368, 828
Bond, J. R., Kofman, L., & Pogosyan, D. 1996, Nature, 380, 603
Boselli, A., & Gavazzi, G. 2006, PASP, 118, 517
Bruzual, G., & Charlot, S. 2003, MNRAS, 344, 1000
Cantiello, M., Blakeslee, J. P., Raimondo, G., Mei, S., Brocato, E., & Capaccioli, M. 2005, ApJ, 634, 239
Cantiello, M., Raimondo, G., Brocato, E., & Capaccioli, M. 2003, AJ, 125, 2783
Côté, P., McLaughlin, D. E., Cohen, J. G., & Blakeslee, J. P. 2003, ApJ, 591, 850
Côté, P., et al. 2001, ApJ, 559, 828
———. 2004, ApJS, 153, 223 (Paper I)
———. 2006, ApJS, 165, 57 (Paper VIII)
de Vaucouleurs, G. 1961, ApJS, 6, 213
de Vaucouleurs, G., & de Vaucouleurs, A. 1973, A&A, 28, 109
Dressler, A., & Shectman, S. A. 1988, AJ, 95, 985
Dunn, L. P., & Jerjen, H. 2006, AJ, 132, 1384
Federspiel, M. Tammann, G. A., & Sandage, A. 1998, ApJ, 495, 115
Ferrarese, L., et al. 1996, ApJ, 464, 568
———. 2006a, ApJS, 164, 334 (Paper VI)
———. 2006b, ApJ, 644, L21
Fitchett, M., & Webster, R. 1987, ApJ, 317, 653
Fukugita, M., Okamura, S., & Yasuda, N. 1993, ApJ, 412, L13

Freedman, W. L., et al. 1994, Nature, 371, 757
———. 2001, ApJ, 553, 47
Fouqué, P., Solanes, J. M., Sanchis, T., & Balkowski, C. 2001, A&A, 375, 770
Gavazzi, G., Boselli, A., Scodeggio, M., Pierini, D., & Belsole, E. 1999, MNRAS, 304, 595
Geller, M. J., & Beers, T. C. 1982, PASP, 94, 421
Gibson, B. K., et al. 1999, ApJ, 512, 48
Graham, J. A., et al. 1999, ApJ, 516, 626
Haşegan, M., et al. 2005, ApJ, 627, 203 (Paper VII)
Helou, G., Salpeter, E. E., & Krumm, N. 1979, ApJ, 228, L1
Hoffman, G. L., Lewis, B. M., & Salpeter, E. E. 1995, ApJ, 441, 28
Huchra, J. P. 1985, ESO Workshop on the Virgo Cluster, ed. O.-G. Richter & B. Binggeli (Garching: ESO), 181
Jacoby, G. H., et al. 1992, PASP, 104, 599
Jensen, J. B., Tonry, J. L., Barris, B. J., Thompson, R. I., Liu, M. C., Rieke, M. J., Ajhar, E. A., & Blakeslee, J. P. 2003, ApJ, 583, 712
Jensen, J. B., Tonry, J. L., & Luppino, G. A. 1998, ApJ, 505, 111
———. 1999, ApJ, 510, 71
Jerjen, H., Binggeli, B., & Barazza, F. D. 2004, AJ, 127, 771
Jerjen, H., Rekola, R., Takalo, L., Coleman, M., & Valtonen, M. 2001, A&A, 380, 90
Jordán, A., et al. 2004a, ApJS, 154, 509 (Paper II)
———. 2004b, ApJ, 613, 279 (Paper III)
———. 2005a, ApJ, 634, 1002 (Paper X)
———. 2005b, in IAU Colloq. 198, Near-Fields Cosmology with Dwarf Elliptical Galaxies, ed. H. Jerjen & B. Binggeli (Cambridge: Cambridge Univ. Press), 368
———. 2006a, ApJ, 651, L25
———. 2006b, ApJS, submitted (Paper XII)
Liu, M. C., & Graham, J. R. 2001, ApJ, 557, L31
Liu, M. C., Graham, J. R., & Charlot, S. 2002, ApJ, 564, 216
Macri, L. M., et al. 1999, ApJ, 521, 155
McLaughlin, D. E. 1999, ApJ, 512, L9
Mei, S., Silva, D. R., & Quinn, P. J. 2001, A&A, 366, 54
Mei, S., Scodeggio, M., Silva, D.R, & Quinn, P. J. 2003, A&A, 399, 441
Mei, S., et al. 2005a, ApJS, 156, 113 (Paper IV)
———. 2005b, ApJ, 625, 121 (Paper V)
Mellier, Y., Mathez, G., Mazure, A., Chauvineau, B., & Proust, D. 1988, A&A, 199, 67
Merritt, D. 1987, ApJ, 313, 121

Mieske, S., Hilker, M., & Infante, L. 2003, A&A, 403, 43
———. 2006a, A&A, 458, 1013
———. 2006b, ApJ, 653, 193
Mohr, J. J., Fabricant, D. G., & Geller, M. J. 1993, ApJ, 413, 492
Neilsen, E. H., & Tsvetanov, Z. I. 2000, ApJ, 536, 255
Oegerle, W. R., & Hill, J. M. 2001, AJ, 122, 2858
Pahre, M. A., & Mould, J. R. 1994, ApJ, 433, 567
Peng, E. W., et al. 2006a, ApJ, 639, 95 (Paper IX)
———. 2006b, ApJ, 639, 838 (Paper XI)
Pierce, M. J., & Tully, B. 1988, ApJ, 330, 579
Pierce, M. J., Welch, D. L., McClure, R. D., van den Bergh, S., Racine, R., & Stetson, P. B. 1994, Nature, 371, 385
Press, W. H., et al. 1992, Numerical Recipes: The Art of Scientific Computing (Cambridge: Cambridge Univ. Press)
Saha, A., Labhardt, L., Schwengeler, H., Macchetto, F. D., Panagia, N., Sandage, A., & Tammann, G. A. 1994, ApJ, 425, 14
Saha, A., Sandage, A., Labhardt, L., Tammann, G. A., Macchetto, F. D., & Panagia, N. 1996, ApJS, 107, 693
———. 1997, ApJ, 486, 1
Sakai, S., et al. 2000, ApJ, 529, 698
Sandage, A., & Tammann, G. A. 1976, ApJ, 207, L1
Schindler, S., Binggeli, B., & Böhringer, H. 1999, A&A, 343, 420
Solanes, J. M.; Sanchis, T., Salvador-Solé, E., Giovanelli, R., & Haynes, M. P. 2002, AJ, 124, 2440

Spergel, D. N., et al. 2006, ApJ, submitted (astro-ph/0603449)
Springel, V., et al. 2005, MNRAS, 361, 776
Struble, M. F., & Rood, H. J. 1999, ApJS, 125, 35
Tanaka, K. I. 1985, PASJ, 37, 133
Tonry, J. L., Ajhar, E. A., & Luppino, G. A. 1990, AJ, 100, 1416
Tonry, J. L., Blakeslee, J. P., Ajhar, E. A., & Dressler, A. 1997, ApJ, 475, 399
———. 2000, ApJ, 530, 625
Tonry, J. L., Dressler, A., Blakeslee, J. P., Ajhar, E. A., Fletcher, A. B., Luppino, G. A., Metzger, M. R., & Moore, C. B. 2001, ApJ, 546, 681
Tonry, J. L., & Schneider, D. P. 1988, AJ, 96, 807
Tully, R. B. 1982, ApJ, 257, 389
Tully, R. B., & Pierce, M. J. 2000, ApJ, 533, 744
Tully, R. B., & Shaya, E. 1984, ApJ, 281, 31
Udalski, A., Soszynski, I., Szymanski, M., Kubiak, M., Pietrzynski, G., Wozniak, P., & Zebrun, K. 1999, Acta Astron., 49, 223
van Haarlem, M., & van de Weygaert, R. 1993, ApJ, 418, 544
West, M. J., & Blakeslee, J. P. 2000, ApJ, 543, L27
West, M. J., Jones, C., & Forman, W. 1995, ApJ, 451, L5
Worthey, G. 1994, ApJS, 95, 107
Yasuda, N., Fukugita, M., & Okamura, S. 1997, ApJS, 108, 417
Young, C. K., & Currie, M. J. 1995, MNRAS, 273, 1141